RESEARCH ARTICLE

PTP1B Is an Intracellular Checkpoint that Limits T-cell and CAR T-cell Antitumor Immunity

Florian Wiede[1,2,3], Kun-Hui Lu[3,4], Xin Du[3,4], Mara N. Zeissig[1,2], Rachel Xu[1,2], Pei Kee Goh[1,2], Chrysovalantou E. Xirouchaki[1,2], Samuel J. Hogarth[1,2], Spencer Greatorex[1,2], Kevin Sek[3,4], Roger J. Daly[1,2], Paul A. Beavis[3,4], Phillip K. Darcy[3,4], Nicholas K. Tonks[5], and Tony Tiganis[1,2,3]

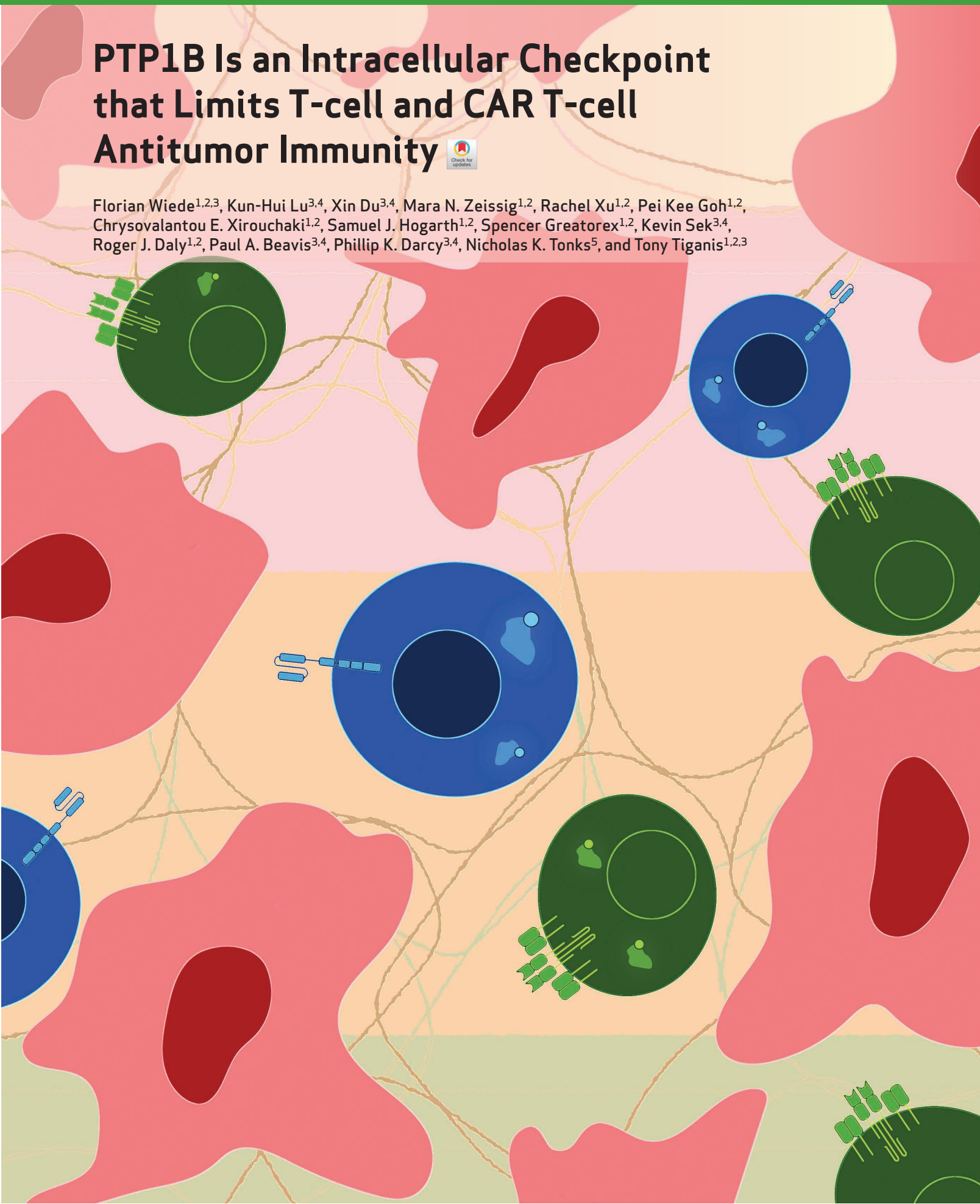

ABSTRACT Immunotherapies aimed at alleviating the inhibitory constraints on T cells have revolutionized cancer management. To date, these have focused on the blockade of cell-surface checkpoints such as PD-1. Herein we identify protein tyrosine phosphatase 1B (PTP1B) as an intracellular checkpoint that is upregulated in T cells in tumors. We show that increased PTP1B limits T-cell expansion and cytotoxicity to contribute to tumor growth. T cell–specific PTP1B deletion increased STAT5 signaling, and this enhanced the antigen-induced expansion and cytotoxicity of $CD8^+$ T cells to suppress tumor growth. The pharmacologic inhibition of PTP1B recapitulated the T cell–mediated repression of tumor growth and enhanced the response to PD-1 blockade. Furthermore, the deletion or inhibition of PTP1B enhanced the efficacy of adoptively transferred chimeric antigen receptor (CAR) T cells against solid tumors. Our findings identify PTP1B as an intracellular checkpoint whose inhibition can alleviate the inhibitory constraints on T cells and CAR T cells to combat cancer.

SIGNIFICANCE: Tumors subvert antitumor immunity by engaging checkpoints that promote T-cell exhaustion. Here we identify PTP1B as an intracellular checkpoint and therapeutic target. We show that PTP1B is upregulated in intratumoral T cells and that its deletion or inhibition enhances T-cell antitumor activity and increases CAR T-cell effectiveness against solid tumors.

INTRODUCTION

Immune checkpoints are crucial for modulating the magnitude of immune responses to minimize collateral tissue damage and overt autoimmunity during antimicrobial defense and T-cell homeostasis (1). Tumors hijack immune checkpoints by upregulating their cell-surface ligands for T cell–inhibitory receptors. In particular, the inflammatory tumor microenvironment is instrumental in driving the expression of ligands, such as PD-L1, which engage T cell–inhibitory receptors, such as PD-1. The engagement of PD-1 on activated T cells by PD-L1 on tumor cells or other cells in the tumor microenvironment suppresses antitumor responses and promotes T-cell exhaustion, a state of deteriorated T-cell function (1, 2). Antibodies blocking the PD-1 immune checkpoint have revolutionized cancer therapy, resulting in durable clinical responses, especially in immunogenic tumors with abundant T-cell infiltrates (3). However, not all tumors are responsive to PD-1 checkpoint blockade, and both primary and adaptive resistance can occur (3). An alternative approach to alleviate the inhibitory constraints on T cells and to overcome T-cell exhaustion in the tumor microenvironment may be to target protein tyrosine phosphatases (PTP) that antagonize T-cell function (4). Such PTPs might include the closely related SHP-1 and SHP-2 that are thought to act redundantly to mediate PD-1–inhibitory signaling in T cells (5, 6), or TCPTP (also known as PTPN2), which antagonizes T-cell receptor (TCR) and cytokine signaling to maintain T-cell tolerance (7–10) and whose deletion enhances both T cell–mediated immune surveillance and the antitumor activity of adoptively transferred T cells (11, 12).

The prototypic tyrosine-specific phosphatase PTP1B (encoded by *PTPN1*) is expressed ubiquitously and has been implicated in various physiologic and pathologic processes (13). PTP1B shares a high degree of structural and sequence identity with TCPTP, and the two phosphatases can function together to coordinate diverse biological processes (13), including, for example, the central nervous system (CNS) control of energy and glucose homeostasis (14, 15). However, it remains unknown whether PTP1B has a role in T cells. PTP1B is fundamentally important in metabolism, and its global deletion results in obesity resistance and improved glucose homeostasis, attributable to the promotion of CNS leptin and peripheral insulin signaling, respectively (16–18). As such, PTP1B has long been considered an exciting therapeutic target for combating metabolic syndrome (13). Indeed, its systemic inhibition with trodusquemine (MSI-1436), a specific allosteric inhibitor of PTP1B (19), promotes weight loss and improves glucose homeostasis in mice (19, 20). Yet, other studies have shown that the inhibition of PTP1B with MSI-1436 might also be useful for the treatment of neurologic disorders, including Rett syndrome (21). Moreover, several studies point toward PTP1B serving as a potential therapeutic target in solid tumors (19, 22–24). In particular, PTP1B levels are elevated in breast cancer, where it is

[1]Monash Biomedicine Discovery Institute, Monash University, Clayton, Victoria, Australia. [2]Department of Biochemistry and Molecular Biology, Monash University, Clayton, Victoria, Australia. [3]Cancer Immunology Program, Peter MacCallum Cancer Centre, Melbourne, Victoria, Australia. [4]Sir Peter MacCallum Department of Oncology, The University of Melbourne, Parkville, Victoria, Australia. [5]Cold Spring Harbor Laboratory, Cold Spring Harbor, New York.

Note: Supplementary data for this article are available at Cancer Discovery Online (http://cancerdiscovery.aacrjournals.org/).

Corresponding Author: Tony Tiganis, Monash Biomedicine Discovery Institute, 23 Innovation Walk, Monash University, Victoria 3800, Australia. Phone: 614-1739-6512; E-mail: Tony.Tiganis@monash.edu

Cancer Discov 2022;12:752–73

doi: 10.1158/2159-8290.CD-21-0694

thought to contribute to tumor growth (22, 23). Consistent with this, the global deletion of PTP1B attenuates the development of mammary tumors driven by mutant ErbB2 in mice (22, 23), whereas MSI-1436 attenuates the growth of xenografts in SCID-beige mice and the metastasis of ErbB2-driven mammary tumors in transgenic (TG) mice (19). These studies have focused on the cell-autonomous contributions of PTP1B in breast cancer tumorigenesis. However, the extent to which PTP1B may affect tumor growth by eliciting non–cell-autonomous effects remains unclear. Although PTP1B heterozygosity has been reported to attenuate the growth of syngeneic Eμ-myc–driven lymphomas in mice by enhancing the immunogenicity of antigen-presenting dendritic cells (DC), paradoxically its complete deletion impairs DC maturation and function (25, 26). Therefore, it remains unclear whether the systemic inhibition of PTP1B might enhance or otherwise repress antitumor immunity.

Cytokine-induced JAK/STAT signaling is fundamentally important for all aspects of immunity (27). In T cells, the induction of STAT5 signaling downstream of common γ (γc) chain cytokines, such as IL2, is essential for T-cell activation, homeostasis, survival, and memory formation (28). It is well established that PTP1B can attenuate JAK/STAT signaling by dephosphorylating and inactivating JAK2 and TYK2 (29, 30). In this study, we show that PTP1B attenuates JAK/STAT5 signaling and antagonizes the expansion and activation of T cells. We show that PTP1B abundance is increased in intratumoral $CD8^+$ T cells to repress antitumor immunity. Using genetic approaches, we establish that the deletion of PTP1B in T cells promotes STAT5 signaling to facilitate the antigen-induced expansion, activation, and cytotoxicity of $CD8^+$ T cells to attenuate the growth of solid tumors. Importantly, we report that inhibition of PTP1B in T cells enhances not only endogenous T cell–mediated antitumor immunity and the response to anti–PD-1 therapy, but also the efficacy of adoptively transferred T cells and CAR T cells to repress the growth of solid tumors. Our findings define a novel intracellular checkpoint and actionable therapeutic target for enhancing the antitumor activity of T cells.

RESULTS

PTP1B Deletion in the Hematopoietic Compartment Represses Solid Tumor Growth

To explore whether PTP1B may elicit non–cell-autonomous effects on the growth of tumors, we generated syngeneic mammary tumors by implanting ovalbumin (OVA)-expressing AT3 (AT3-OVA) murine mammary tumor cells into the inguinal mammary fat pads of *Ptpn1*$^{+/+}$, *Ptpn1*$^{+/-}$ or *Ptpn1*$^{-/-}$ C57BL/6 mice (17) and assessed tumor growth (Fig. 1A and B). We found that mammary tumor growth was markedly attenuated in *Ptpn1*$^{-/-}$ mice so that the resultant tumors were less than half the size of those in *Ptpn1*$^{+/+}$ control mice; intermediate effects were seen in *Ptpn1*$^{+/-}$ C57BL/6 mice, indicating that even partial PTP1B deficiency is sufficient to attenuate tumor growth. The repression of tumor growth was accompanied by an increased abundance of tumor-infiltrating lymphocytes (TIL; Fig. 1C), which in many tumors, including breast cancer, are associated with improved survival and response to therapy (31). These TILs were predominantly $CD44^{hi}CD62L^{lo}$ (CD44 marks activated T cells and CD62L lymphoid-resident T cells; refs. 32, 33) effector/memory $CD8^+$ T cells, which can repress tumor growth (Fig. 1C; Supplementary Fig. S1A), but also included $CD4^+$ T cells, natural killer (NK) cells, and DCs (Fig. 1C), which promote antitumor immunity (3, 34). In addition, the global deletion of PTP1B was accompanied by the recruitment of $CD4^+$ regulatory T cells (Treg), tumor-associated macrophages (TAM), and both granulocytic and monocytic myeloid-derived suppressor cells (MDSC; Fig. 1C; Supplementary Fig. S1B), which are immunosuppressive (3). To determine the extent to which the repression of syngeneic tumor growth may be ascribed to stromal differences, changes in the hormonal milieu, or differences in the hematopoietic compartment, we repeated these experiments using chimeric mice; lethally irradiated $Ly5.1^+$ C57BL/6 recipient mice were reconstituted with congenically marked $Ly5.2^+$ *Ptpn1*$^{+/+}$ control or *Ptpn1*$^{-/-}$ bone marrow before the implantation of AT3-OVA tumor cells into the inguinal mammary fat pads (Fig. 1D). We found that PTP1B deficiency in the hematopoietic compartment alone completely phenocopied the effects of global PTP1B deletion on the repression of tumor growth (Fig. 1E) and the abundance of TILs (Fig. 1F). Therefore, the deletion of PTP1B in the immune compartment is sufficient to increase TILs and suppress tumor growth.

PTP1B Is Increased in Tumor T Cells

Although PTP1B deficiency may potentially affect both innate and adaptive immune compartments to promote antitumor immunity, we focused our attention on $CD8^+$ T cells because they were the most abundantly represented TILs in syngeneic tumors in PTP1B-deficient mice (Fig. 1C). As PTP1B's function in T cells remains unknown, we first assessed its expression in lymphoid versus intratumoral T cells. To this end, we adoptively transferred congenically marked ($Ly5.2^+$) naïve ($CD44^{lo}CD62L^{hi}$) $CD8^+$ T cells expressing the OT-I TCR, which is specific for OVA, into immunocompetent $Ly5.1^+$ mice bearing AT3-OVA mammary tumors and assessed PTP1B protein in both the endogenous and adoptively transferred $CD8^+$ T-cell subsets in the spleens versus tumors by flow cytometry (Fig. 2A; Supplementary Fig. S2; see Supplementary Fig. S3 for gating strategy). Endogenous splenic T cells from tumor-bearing mice were largely naïve in phenotype, but also included a smaller proportion of $CD44^{hi}CD62L^{hi}$ central memory and $CD44^{hi}CD62L^{lo}$ effector/memory T cells (Supplementary Fig. S3). By contrast, adoptively transferred OT-I T cells had central memory or effector/memory phenotypes in spleens and an effector/memory phenotype in tumors (Supplementary Fig. S3); the central memory and effector/memory OT-I T cells in the spleens of tumor-bearing mice likely originated from adoptively transferred naïve T cells that had engaged antigen and had recirculated from the tumor to lymphoid organs (32, 33). In endogenous splenic $CD8^+$ T cells, PTP1B protein as assessed by flow cytometry was moderately elevated in central memory and effector/memory T cells when compared with naïve T cells (Fig. 2A). By contrast, PTP1B protein was elevated by approximately twofold in both endogenous effector/memory $CD8^+$ T cells and adoptively transferred OT-I effector/memory T cells in tumors when compared with the corresponding effector/memory T cells in spleens (Fig. 2A);

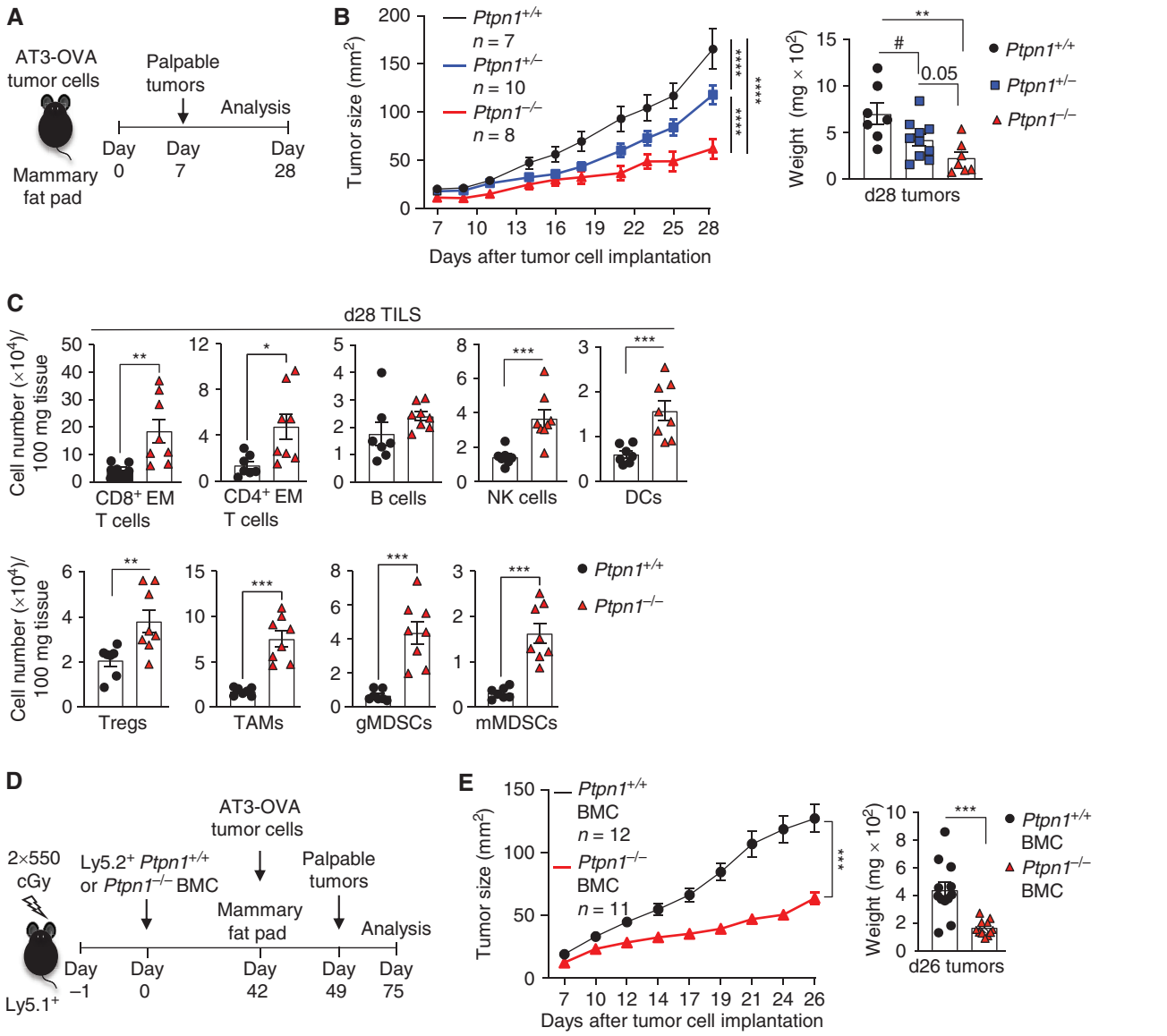

Figure 1. PTP1B deletion in immune cells enhances antitumor immunity. **A–C,** AT3-OVA tumor cells were implanted into the fourth inguinal mammary fat pads of *Ptpn1*$^{+/+}$, *Ptpn1*$^{+/-}$, or *Ptpn1*$^{-/-}$ littermate mice, and tumor growth and weights were measured. **C,** TILs including CD44^{hi}CD62L^{lo} CD8$^+$ and CD4$^+$ effector/memory (EM) T cells, B220$^+$ B cells, NK1.1$^+$TCRβ$^-$ (natural killer, NK) cells, CD11c$^+$ DCs, CD4$^+$CD25$^+$FoxP3$^+$ regulatory T cells (Treg), CD11b$^+$F4/80^{hi}Ly6C$^-$Ly6G$^-$ tumor-associated macrophages (TAM), granulocytic CD11b$^+$F4/80$^{hi/lo}$ Ly6C^{int}Ly6G$^+$ myeloid-derived suppressor cells (gMDSC), and monocytic CD11b$^+$F4/80$^{hi/lo}$ Ly6C$^+$Ly6G$^-$ myeloid-derived suppressor cells (mMDSC) were analyzed by flow cytometry. **D** and **E,** Lethally irradiated Ly5.1 mice were reconstituted with bone marrow cells derived from *Ptpn1*$^{+/+}$ or *Ptpn1*$^{-/-}$ mice. After 4 weeks of reconstitution, AT3-OVA tumor cells were implanted into the fourth inguinal mammary fat pads of PTP1B-deficient or control bone marrow chimeras (BMC) and tumor growth monitored, final weights measured, and tumor infiltration (**F**) analyzed by flow cytometry. Representative results (means ± SEM) from at least two independent experiments are shown. Significance was determined as follows: tumor sizes in **B** and **E** (two-way ANOVA test), tumor weights in **B** and **E** and immune cell infiltrates in **C** and **F** (two-tailed Mann–Whitney *U* test or one-way ANOVA test), and tumor weights in **B** [two-tailed Mann–Whitney *U* test (#, $P < 0.05$)]. *, $P < 0.05$; **, $P < 0.01$; ***, $P < 0.001$; ****, $P < 0.0001$.

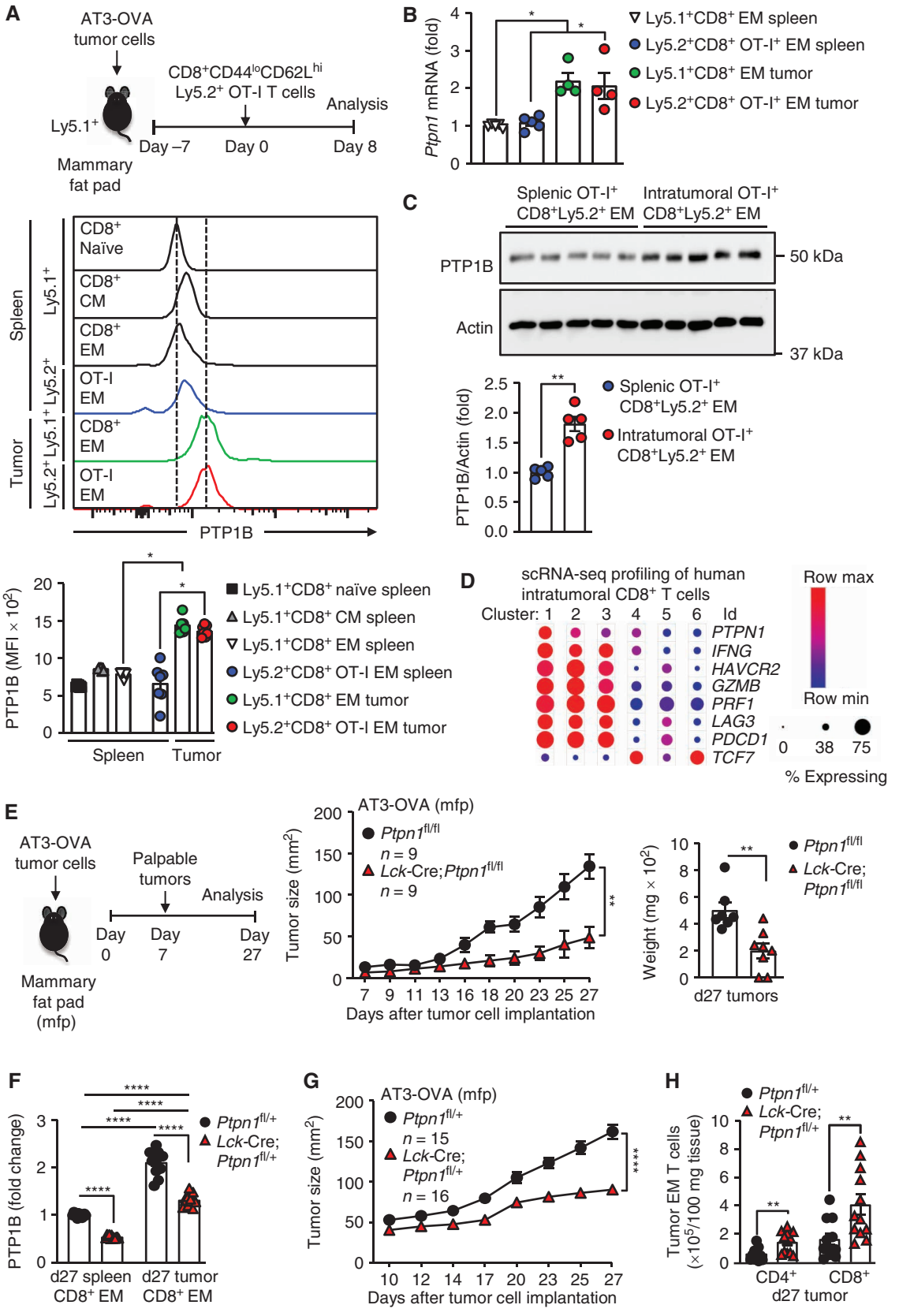
A
AT3-OVA tumor cells
CD8+CD44loCD62Lhi Ly5.2+ OT-I T cells
Analysis
Ly5.1+
Day –7
Day 0
Day 8
Mammary fat pad
Spleen
Tumor
Ly5.1+
Ly5.2+ Ly5.1+
Ly5.2+
CD8+ Naïve
CD8+ CM
CD8+ EM
OT-I EM
CD8+ EM
OT-I EM
PTP1B
B
Ptpn1 mRNA (fold)
Ly5.1+CD8+ EM spleen
Ly5.2+CD8+ OT-I+ EM spleen
Ly5.1+CD8+ EM tumor
Ly5.2+CD8+ OT-I+ EM tumor
C
Splenic OT-I+ CD8+Ly5.2+ EM
Intratumoral OT-I+ CD8+Ly5.2+ EM
PTP1B
Actin
50 kDa
37 kDa
PTP1B/Actin (fold)
Splenic OT-I+ CD8+Ly5.2+ EM
Intratumoral OT-I+ CD8+Ly5.2+ EM
PTP1B (MFI × 10²)
Ly5.1+CD8+ naïve spleen
Ly5.1+CD8+ CM spleen
Ly5.1+CD8+ EM spleen
Ly5.2+CD8+ OT-I EM spleen
Ly5.1+CD8+ EM tumor
Ly5.2+CD8+ OT-I EM tumor
Spleen
Tumor
D
scRNA-seq profiling of human intratumoral CD8+ T cells
Cluster: 1 2 3 4 5 6
Id
PTPN1
IFNG
HAVCR2
GZMB
PRF1
LAG3
PDCD1
TCF7
Row max
Row min
0 38 75
% Expressing
E
AT3-OVA tumor cells
Palpable tumors
Analysis
Day 0
Day 7
Day 27
Mammary fat pad (mfp)
AT3-OVA (mfp)
Ptpn1fl/fl n = 9
Lck-Cre;Ptpn1fl/fl n = 9
Tumor size (mm²)
Days after tumor cell implantation
Weight (mg × 10²)
d27 tumors
Ptpn1fl/fl
Lck-Cre; Ptpn1fl/fl
F
PTP1B (fold change)
d27 spleen CD8+ EM
d27 tumor CD8+ EM
Ptpn1fl/+
Lck-Cre; Ptpn1fl/+
G
AT3-OVA (mfp)
Ptpn1fl/+ n = 15
Lck-Cre; Ptpn1fl/+ n = 16
Tumor size (mm²)
Days after tumor cell implantation
H
Ptpn1fl/+
Lck-Cre; Ptpn1fl/+
Tumor EM T cells (×10⁵/100 mg tissue)
CD4+ d27 tumor
CD8+ d27 tumor

the increased PTP1B protein in intratumoral versus splenic effector/memory T cells was accompanied by increased *Ptpn1* mRNA expression, as assessed by quantitative real-time PCR (Fig. 2B). Moreover, PTP1B protein, as assessed by immunoblotting, was elevated more than twofold in tumor effector/memory OT-I T cells when compared with splenic effector/memory OT-I T cells (Fig. 2C). Therefore, PTP1B levels are elevated in intratumoral T cells, and the induction of PTP1B is not an outcome of T-cell differentiation or activation, but rather an outcome of conditions within the tumor microenvironment. In line with our findings in mice, an analysis of publicly available single-cell RNA-sequencing data of immune cells isolated from the tumors of patients with melanoma revealed that *PTPN1* mRNA was increased in human intratumoral CD8$^+$ T cells with an effector [high for interferon (IFN) γ (*IFNG*), granzyme B (*GZMB*), and perforin (*PRF1*)] or exhausted [high for TIM3 (*HAVCR2*), LAG3 (*LAG3*), and PD-1 (*PDCD1*)] phenotype (Fig. 2D), otherwise associated with a poor response to PD-1 checkpoint blockade (35), as compared with PTP1B levels in intratumoral T cells with a stem cell or memory phenotype (high for *TCF7*; Fig. 2D), which is associated with a positive clinical outcome to PD-1 blockade (35). This suggests that, as in murine models, PTP1B levels are elevated in human intratumoral T cells and may negatively regulate T-cell responses and the response to immunotherapy.

PTP1B Deletion Enhances T-cell Antitumor Immunity

To explore whether the induction of PTP1B in intratumoral T cells might limit T-cell function and antitumor immunity, and if enhanced T-cell responses in *Ptpn1*$^{-/-}$ mice might contribute to the repression of tumor growth, we sought to delete PTP1B in T cells using the *Lck*-Cre transgene; the *Lck*-Cre transgene specifically deletes floxed alleles at the early stages of T-cell development in the thymus (7). As expected, PTP1B was reduced in total thymocytes and efficiently deleted in T cells, but not myeloid cells, B cells, or nonlymphoid organs (Supplementary Figs. S4 and S5). The T cell–specific deletion of PTP1B increased total thymocyte numbers at each stage of development without affecting positive selection (Supplementary Fig. S6A–S6E) and resulted in increased peripheral naïve, effector/memory, and central memory T cells in lymphoid organs (Supplementary Fig. S6F–S6I); the increase in peripheral T-cell numbers was also noted in *Ptpn1*$^{-/-}$ mice with a global deletion in PTP1B (Supplementary Fig. S7A and S7B). The increased T-cell abundance was not associated with overt pathology, including lymphomas or CD4$^+$CD8$^+$CD3$^-$ leukemias, when mice were aged for 1 year (Supplementary Fig. S8A) or 2 years (Supplementary Fig. S8B). Moreover, there were no signs of systemic inflammation or autoimmunity, as assessed by monitoring for lymphocytic infiltrates in nonlymphoid organs (Supplementary Figs. S9A and S9B and S10A and S10B) as well as the presence of inflammatory cytokines and antinuclear antibodies in serum, and there were no signs of tissue damage, as assessed histologically and by monitoring for the presence of the liver enzymes alanine aminotransferase and aspartate aminotransferase in serum (Supplementary Fig. S11A–S11G).

To assess the influence of PTP1B deletion on T cell–mediated antitumor immunity, we implanted AT3-OVA mammary tumor cells (36) into the inguinal mammary fat pads of control (*Ptpn1*$^{fl/fl}$) and T cell–specific PTP1B-deficient (*Lck*-Cre;*Ptpn1*$^{fl/fl}$) female mice (Fig. 2E). We found that the growth of orthotopic AT3-OVA mammary tumors was significantly repressed (Fig. 2E), and this was associated with a significant improvement in survival (Supplementary Fig. S12A); notably, the repression of AT3-OVA mammary tumor growth paralleled that in *Ptpn1*$^{-/-}$ mice consistent with the repression of tumor growth in *Ptpn1*$^{-/-}$ mice (Fig. 1A) being T cell–dependent. Indeed, the repression of tumor growth in *Lck*-Cre;*Ptpn1*$^{fl/fl}$ mice was accompanied by the accumulation of effector/memory CD4$^+$ and CD8$^+$ T cells (Supplementary Fig. S12B), consistent with T cell–mediated tumor eradication; no overt differences in tumor cell proliferation or apoptosis or tumor angiogenesis were evident (Supplementary Fig. S13). The deletion of PTP1B also significantly repressed the growth of other syngeneic tumors, including OVA-expressing B16F10 (B16F10-OVA) melanoma cells (Supplementary Fig. S14A) and MC38 (MC38-OVA) colorectal cancer cells (Supplementary Fig. S14B and S14C) implanted into the flanks of male mice. Moreover, the deletion of PTP1B in *Lck*-Cre;*Ptpn1*$^{fl/fl}$ mice also repressed the growth of non–OVA-expressing AT3, B16F10 and MC38 syngeneic tumors (Supplementary Fig. S15A–S15E), and the repression of tumor growth was similarly accompanied by the accumulation of effector/memory T cells (Supplementary Fig. S15B); in contrast, the *Lck*-Cre transgene alone had no effect on syngeneic tumor growth (Supplementary Fig. S16). Therefore, PTP1B deficiency can enhance T cell–mediated antitumor immunity, irrespective of whether tumors are overtly immunogenic and express OVA.

Figure 2. Increased PTP1B in intratumoral CD8$^+$ T cells limits antitumor immunity. **A–C,** Naïve (CD44^{lo}CD62L^{hi}) Ly5.2$^+$CD8$^+$OT-I$^+$ cells from OT-I;*Ptpn1*$^{fl/fl}$ or T cell–specific PTP1B-deficient OT-I;*Lck*-Cre;*Ptpn1*$^{fl/fl}$ mice were adoptively transferred into Ly5.1 mice bearing established (40–50 mm^2) AT3-OVA mammary tumors. **A,** Eight days after adoptive transfer, PTP1B protein levels were determined by flow cytometry in splenic or intratumoral Ly5.1$^+$CD8$^+$ recipient or Ly5.2$^+$CD8$^+$OT-I$^+$ donor T cells with a naïve, central/memory (CM; CD44^{hi}CD62L^{hi}), or effector/memory (EM; CD44^{hi}CD62L^{lo}) phenotype. MFI, mean fluorescence intensity. **B,** *Ptpn1* mRNA in FACS-purified splenic and intratumoral Ly5.1$^+$CD8$^+$ recipient and Ly5.2$^+$OT-I$^+$CD8$^+$ donor effector/memory T cells isolated on day 5 after adoptive transfer was assessed by quantitative real-time PCR. **C,** PTP1B protein levels in FACS-purified splenic and intratumoral Ly5.2$^+$CD8$^+$OT-I$^+$ donor effector/memory T cells isolated on day 8 after adoptive transfer were assessed by immunoblotting. **D,** The Broad Institute Single Cell Portal (https://singlecell.broadinstitute.org/single_cell) was used to interrogate publicly available single-cell RNA-sequencing (scRNA-seq) data performed on immune cells isolated from 48 tumor biopsies taken from 32 patients with metastatic melanoma treated with checkpoint blockade therapy. Fine clustering of CD8$^+$ T-cell subsets revealed six clusters. **E,** AT3-OVA tumor cells were implanted orthotopically into the fourth inguinal mammary fat pads of control (*Ptpn1*$^{fl/fl}$) mice or T cell–specific PTP1B-deficient (*Lck*-Cre;*Ptpn1*$^{fl/fl}$) mice. Tumor growth was monitored, and final tumor weights were determined. **F** and **G,** AT3-OVA tumor cells were implanted orthotopically into the fourth inguinal mammary fat pads of control (*Ptpn1*$^{fl/+}$) mice or T cell–specific PTP1B heterozygous (*Lck*-Cre;*Ptpn1*$^{fl/+}$) mice, and PTP1B protein levels (**F**) in CD8$^+$ effector/memory T cells were analyzed by flow cytometry. Tumor growth was monitored (**G**), and tumor-infiltrating CD4$^+$ and CD8$^+$ effector/memory T cells (**H**) were analyzed by flow cytometry. Representative results (means ± SEM) from at least two independent experiments are shown. Significance was determined using a one-way ANOVA test in **A** and **F**; a two-tailed Mann–Whitney *U* test in **B**, **C**, and **H**; a two-way ANOVA test in **E** and **G**; and a two-tailed Mann–Whitney *U* test for tumor weight in **E**. *, $P < 0.05$; **, $P < 0.01$; ****, $P < 0.0001$.

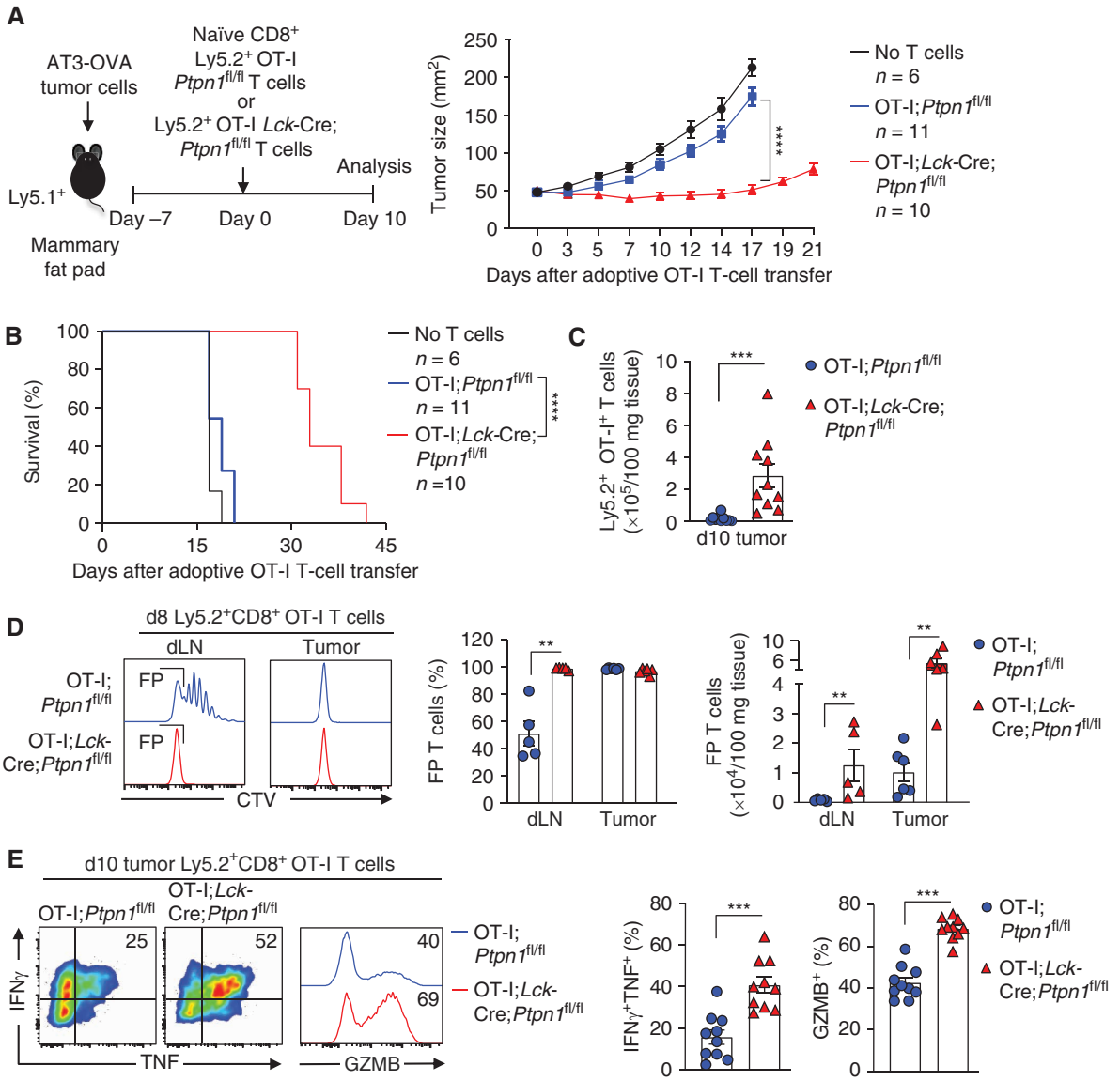

Figure 3. PTP1B deletion in CD8+ T cells enhances antitumor immunity. Naïve (CD44^{lo}CD62L^{hi}) Ly5.2+CD8+OT-I+ T cells from OT-I;*Ptpn1*$^{fl/fl}$ and OT-I; *Lck*-Cre;*Ptpn1*$^{fl/fl}$ mice were adoptively transferred into Ly5.1 mice bearing established (40–50 mm^2) AT3-OVA mammary tumors, and tumor growth (**A**), survival (**B**), and Ly5.2+CD8+ OT-I T-cell infiltrates (**C**; day 10 after adoptive transfer) were determined. **D,** CTV-labeled naïve Ly5.2+CD8+OT-I+ T cells from OT-I;*Ptpn1*$^{fl/fl}$ or OT-I;*Lck*-Cre;*Ptpn1*$^{fl/fl}$ mice were adoptively transferred into Ly5.1 mice bearing established (40–50 mm^2) AT3-OVA mammary tumors and fast proliferating (FP) T cells monitored in the draining lymph nodes (dLN) and tumors. **E,** Tumor-infiltrating T cells from **C** were stimulated with phorbol 12-myristate 13-acetate/ionomycin in the presence of Golgi Stop/Plug and stained for intracellular IFNγ and TNF. Intracellular GZMB was detected in unstimulated tumor-infiltrating CD8+ T cells. For tumor growth in **A**, significance was determined using a two-way ANOVA test. For tumor T-cell infiltrates in **C** and **D** and for intracellular IFNγ, TNF, and GZMB levels in **E**, significance was determined using a two-tailed Mann–Whitney *U* test. In **B**, significance was determined using the log-rank (Mantel–Cox) test. **, $P < 0.01$; ***, $P < 0.001$; ****, $P < 0.0001$.

As PTP1B was induced by approximately twofold in intratumoral T cells (Fig. 2B and C), we next assessed whether the heterozygous deletion of PTP1B in T cells might be sufficient to alleviate the inhibitory effects on T-cell function and enhance antitumor immunity. We found that PTP1B heterozygosity largely corrected the increased PTP1B in intratumoral T cells (Fig. 2F) and repressed the growth of AT3-OVA mammary tumors in *Lck*-Cre;*Ptpn1*$^{fl/+}$ mice (Fig. 2G), and this was accompanied by increased CD4+ and CD8+ effector/memory T cells in tumors (Fig. 2H). Taken together these results point toward PTP1B serving as an intracellular checkpoint and its induction repressing T cell–mediated antitumor immunity.

To specifically explore the contributions of CD8+ T cells, we next asked whether the deletion of PTP1B could promote the tumor-specific activity of TG OT-I CD8+ T cells adoptively transferred into mice bearing OVA-expressing tumors. Naïve control (*Ptpn1*$^{fl/fl}$) or PTP1B-deficient (*Lck*-Cre;*Ptpn1*$^{fl/fl}$) congenically marked (Ly5.2+) OT-I CD8+ T cells were adoptively transferred into immunocompetent and nonirradiated (Ly5.1+) C57BL/6 hosts with AT3-OVA mammary tumors (Fig. 3). Adoptively transferred control CD8+ T cells had little

effect on tumor growth (Fig. 3A). By contrast, PTP1B-deficient CD8$^+$ T cells significantly repressed the growth of AT3-OVA mammary tumors (Fig. 3A) and significantly increased the survival of mice (Fig. 3B). The repression of tumor growth was accompanied by an increased abundance of PTP1B-deficient tumor-infiltrating effector/memory T cells (Fig. 3C; Supplementary Fig. S17); no overt differences in tumor cell proliferation or apoptosis or tumor angiogenesis were evident (Supplementary Fig. S18). The increased abundance of T cells was associated with a marked increase in T-cell proliferation in the draining lymph nodes, as reflected by the presence of "fast proliferating" T cells [assessed by the dilution of the fluorescent dye CellTrace Violet (CTV), which defines distinct populations of dividing cells; Fig. 3D]; increased T-cell activation, as assessed by the expression of CD44; and increased cytotoxicity, as assessed by the expression of IFNγ and TNF as well as GZMB (Fig. 3E; Supplementary Fig. S17), which accumulates in cytolytic granules and mediates tumor cell killing when released into the immunologic synapse. These results indicate that PTP1B deficiency in CD8$^+$ T cells enhances the expansion, activation, and cytotoxic activity of CD8$^+$ T cells to repress tumor growth. Moreover, these results are consistent with elevated PTP1B in intratumoral CD8$^+$ T cells repressing T cell–mediated antitumor immunity to facilitate tumor growth.

PTP1B Deletion Promotes STAT5-Dependent T-cell Expansion, Activation, and Antitumor Immunity

To elucidate how PTP1B deficiency promotes T cell–mediated antitumor immunity, we first assessed whether PTP1B deletion might enhance the αβ TCR signaling that is essential for T-cell activation and function (37). We found that PTP1B deficiency did not result in gross changes in protein tyrosine phosphorylation or the activation of canonical TCR signaling intermediates after cross-linking the αβ TCR on naïve CD8$^+$ T cells with anti-CD3ε (Supplementary Fig. S19A–S19D). However, PTP1B deficiency significantly enhanced the TCR-instigated activation of T cells and the generation of effector T cells, as monitored by (i) the increased cell-surface expression of CD44, CD69 and CD25 [IL2 receptor (IL2R) α chain; Fig. 4A; Supplementary Fig. S20A and S20B], markers of T-cell activation, and responsiveness to IL2, and (ii) the decreased expression of CD62L (Fig. 4A; Supplementary Fig. S20A and S20B), which allows for T cells to exit lymphoid organs and act as effectors. PTP1B deletion was also associated with a marked enhancement in naïve CD8$^+$ T-cell proliferation and/or resulted in increased T-cell numbers across a range of α-CD3ε concentrations, as reflected by the dilution of CTV and the number of resultant cells (Fig. 4B; Supplementary Fig. S20C and S20D). The enhanced proliferative capacity was reaffirmed by monitoring the incorporation of BrdU (measures S-phase entry) in α-CD3ε–stimulated T cells (Supplementary Fig. S21A). Importantly, even at saturating α-CD3ε concentrations, when differences in CTV dilution were not evident, PTP1B deficiency resulted in increased cell numbers, consistent with increased survival (Fig. 4B; Supplementary S20C and S20D). In line with this, the deletion of PTP1B was also accompanied by decreased apoptosis in proliferating cells, as assessed by staining for Annexin V (Supplementary Fig. S21B). PTP1B deficiency also enhanced the expansion of naïve OT-I T cells challenged with the cognate OVA peptide SIINFEKL (N4). Importantly, PTP1B deficiency similarly enhanced responses to the altered peptide ligands SIYNFEKL (Y3) or SIIQFEKL (Q4) that have progressively lower affinities (N4>Y3>>Q4) for the OT-I TCR (Supplementary Fig. S22), consistent with PTP1B deficiency promoting T-cell expansion without altering the threshold for TCR-instigated responses. The activation and expansion of naïve T cells is reliant not only on signaling from the TCR (signal 1) and coreceptors such as CD28 (signal 2), but also on cytokines such as IL2 (signal 3; refs. 28, 37). IL2 signals via JAK protein tyrosine kinases (PTK) and STAT5 to drive the expression of genes that are essential for T-cell proliferation, survival, differentiation, and cytotoxicity (28, 38, 39). PTP1B deficiency increased basal STAT5 Y694 phosphorylation (p-STAT5), as monitored by flow cytometry in naïve and central memory T cells, and this was accompanied by an increased abundance of BCL2, which promotes cell survival (Fig. 4C), and of T-bet and Eomes (Fig. 4D), which are transcriptional targets of STAT5 that promote CD8$^+$ T-cell cytotoxicity and CD4$^+$ T-cell differentiation (28). Moreover, PTP1B deficiency enhanced STAT5 signaling in response to IL2 in effector T cells (Fig. 4E), as well as p-STAT5 downstream of IL7 and IL15 in different T-cell subsets (Supplementary Fig. S23). The enhanced p-STAT5 was accompanied by increased TYK2 Y1054/Y1055 phosphorylation (p-TYK2) in response to IL2 and IL15 (Supplementary Fig. S24A). The activation of JAK PTKs by cytokines also results in PI3K/AKT and Ras/MAPK signaling. As expected, PTP1B deletion also enhanced IL2-induced PI3K/AKT signaling (AKT Ser-473 phosphorylation; p-AKT) and Ras/MAPK signaling (phosphorylation of ERK-1/2; p-ERK1/2; Supplementary Fig. S24B). The promotion of STAT5 signaling occurred not only as a consequence of increasing JAK activation, but also as a result of increasing STAT5 phosphorylation, because the inhibition of JAK PTKs with ruxolitinib in T cells pulsed with IL2 was accompanied by prolonged albeit attenuated p-STAT5 (Supplementary Fig. S24C). Therefore, the deletion of PTP1B enhances the activation and expansion of T cells and promotes both JAK and STAT5 signaling, but not TCR signaling.

To assess whether PTP1B might have similar roles in human T cells, we took advantage of CRISPR–Cas9 genome editing to delete PTP1B in T cells derived from human peripheral blood mononuclear cells (PBMC; Supplementary Fig. S25A). As in murine T cells, we found that the deletion of PTP1B resulted in enhanced basal p-STAT5 and the expression of BCL2 family members, including BCL2 and BCL-xL (Supplementary Fig. S25B). PTP1B deletion also enhanced the expansion (as assessed by CTV dilution) and activation (as assessed by CD69 cell-surface levels) of T cells after TCR cross-linking with α-CD3 (Supplementary Fig. S25C and S25D). Therefore, the deletion of PTP1B promotes STAT5 signaling and facilitates the expansion and activation of both murine and human T cells.

Although JAK2 and TYK2 can signal via multiple STATs, the promotion of STAT5 signaling in T cells is essential for proliferation after TCR ligation and for effector T-cell responses (28, 38, 39). To explore the extent to which heightened STAT5 signaling may contribute to the enhanced T-cell expansion

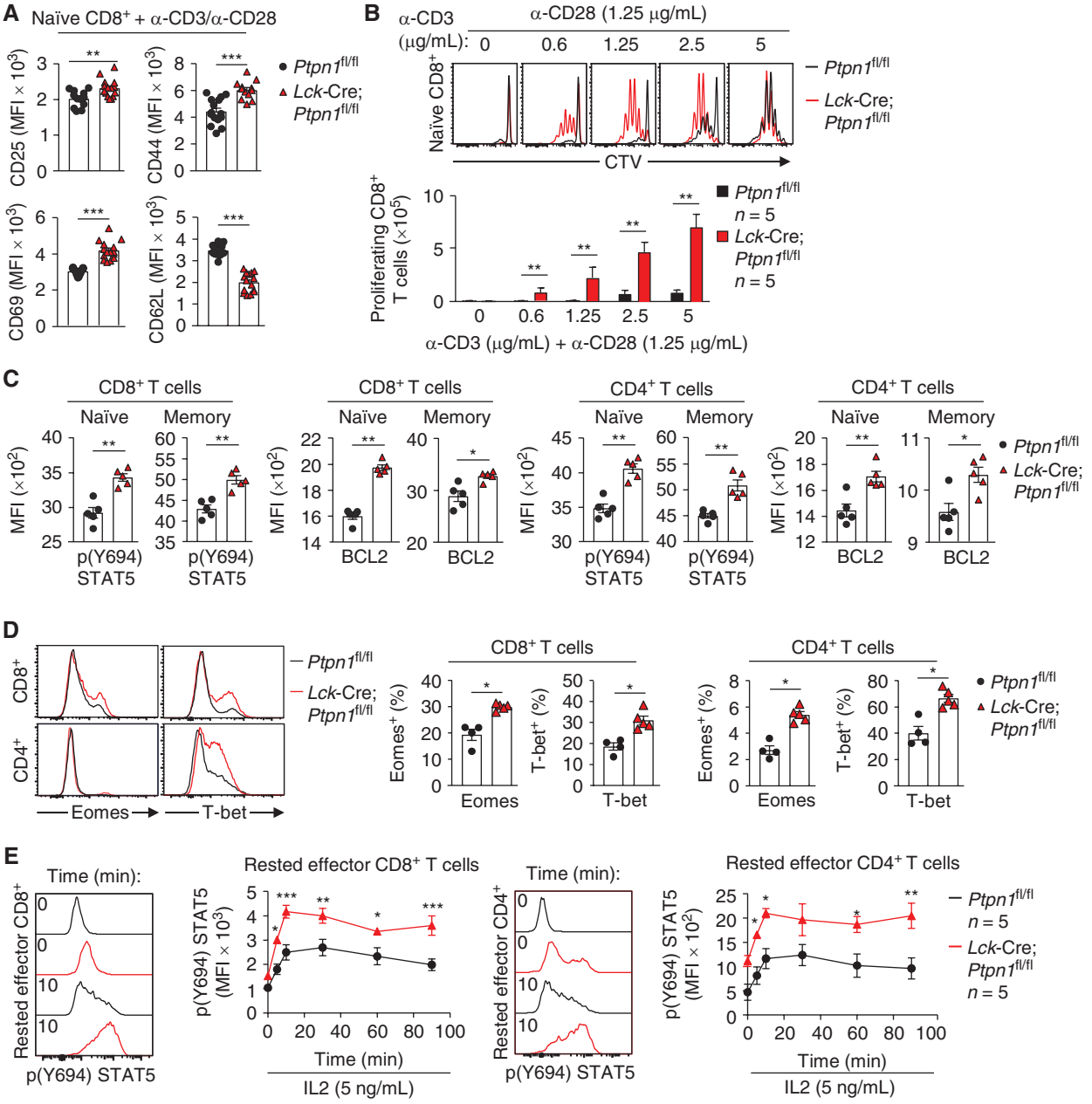

Figure 4. PTP1B deletion enhances T-cell activation, proliferation, survival, and STAT5 signaling. **A,** Naïve (CD44^{lo}CD62L^{hi}) CD8$^+$ T cells from *Ptpn1*$^{fl/fl}$ and *Lck*-Cre;*Ptpn1*$^{fl/fl}$ were stimulated with plate-bound α-CD3 (2.5 μg/mL) and α-CD28 (1.25 μg/mL) for 48 hours and CD25, CD44, CD69, and CD62L levels determined by flow cytometry. **B,** CTV-labeled naïve CD8$^+$ T cells from *Ptpn1*$^{fl/fl}$ and *Lck*-Cre;*Ptpn1*$^{fl/fl}$ mice were stimulated with the indicated concentrations of plate-bound α-CD3 plus α-CD28 (1.25 μg/mL) for 72 hours and T-cell proliferation (CTV dilution) determined by flow cytometry. **C,** Basal intracellular p-STAT5 and BCL2 levels were assessed by flow cytometry in naïve (CD44^{lo}) and memory (CD44^{hi}) CD4$^+$ and CD8$^+$ T cells from *Ptpn1*$^{fl/fl}$ and *Lck*-Cre;*Ptpn1*$^{fl/fl}$ mice. **D,** Intracellular Eomes and T-bet protein levels were assessed by flow cytometry in CD8$^+$ and CD4$^+$ T cells from *Ptpn1*$^{fl/fl}$ and *Lck*-Cre;*Ptpn1*$^{fl/fl}$ mice. **E,** *In vitro*–generated rested effector CD8$^+$ or CD4$^+$ T cells were stimulated with IL2 (5 ng/mL) for the indicated times and intracellular STAT5 Y694 phosphorylation (p-STAT5) assessed by flow cytometry. Representative results (means ± SEM) from at least two independent experiments are shown. Significance in **A**–**D** was determined using a two-tailed Mann–Whitney *U* test and in **E** using a two-way ANOVA test. *, $P < 0.05$; **, $P < 0.01$; ***, $P < 0.001$.

and activation in PTP1B-deficient T cells, we crossed *Lck*-Cre; *Ptpn1*$^{fl/fl}$ mice onto a *Stat5*$^{fl/+}$ heterozygous background to decrease p-STAT5. *Stat5* heterozygosity largely corrected the elevated basal p-STAT5, and the associated increase in BCL2 protein, in naïve and central memory PTP1B-deficient CD4$^+$ and CD8$^+$ T cells (Fig. 5A and B; Supplementary S26A and S26B). Moreover, *Stat5* heterozygosity corrected the increased abundance of peripheral CD4$^+$ and CD8$^+$ naïve and central memory T cells *in vivo* (Supplementary Fig. S26C). Importantly, *Stat5* heterozygosity also largely, if not completely, corrected the enhanced α-CD3ε/α-CD28–induced T-cell activation, as assessed by the correction in CD25, CD44, and

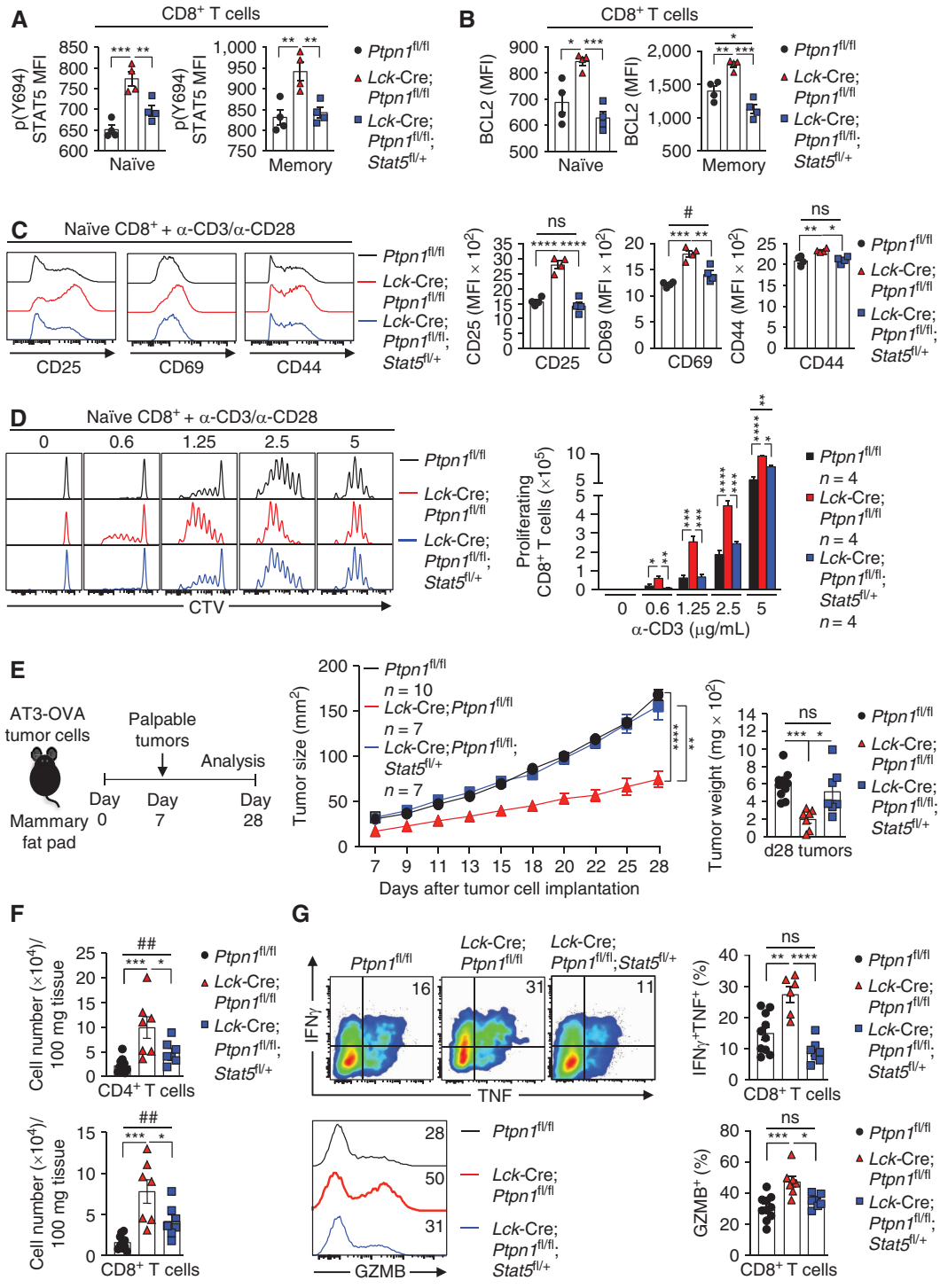

Figure 5. PTP1B deficiency promotes STAT5-dependent T-cell activation and antitumor immunity. Basal intracellular p-STAT5 (**A**) and BCL2 (**B**) levels were assessed in naïve ($CD44^{lo}$) and memory ($CD44^{hi}$) lymph node $CD8^+$ T cells from *Ptpn1*$^{fl/fl}$, *Lck*-Cre;*Ptpn1*$^{fl/fl}$, and *Lck*-Cre;*Ptpn1*$^{fl/fl}$*Stat5*$^{fl/+}$ mice. MFI, mean fluorescence intensity. **C,** Naïve $CD8^+$ ($CD44^{lo}CD62L^{hi}$) T cells were stimulated with plate-bound α-CD3 (2.5 μg/mL) plus α-CD28 (1.25 μg/mL) for 48 hours, and cell-surface CD25, CD44, and CD69 levels (MFIs) were determined. **D,** CTV-labeled naïve $CD8^+$ T cells were stimulated with the indicated concentrations of plate-bound α-CD3 plus α-CD28 (1.25 μg/mL) for 72 hours, and T-cell proliferation (CTV dilution) was assessed by flow cytometry. **E** and **F,** AT3-OVA tumor cells were implanted orthotopically into the fourth inguinal mammary fat pads of *Ptpn1*$^{fl/fl}$, *Lck*-Cre;*Ptpn1*$^{fl/fl}$, or *Lck*-Cre;*Ptpn1*$^{fl/fl}$;*Stat5*$^{fl/+}$ mice (**E**), and tumor growth, final tumor weights, and the number of tumor-infiltrating $CD4^+$ and $CD8^+$ T cells (**F**) were determined. **G,** Intratumoral $CD8^+$ T cells were stimulated with phorbol 12-myristate 13-acetate/ionomycin in the presence of Golgi Stop/Plug and stained for intracellular IFNγ and TNF. Intracellular GZMB was assessed in unstimulated intratumoral $CD8^+$ T cells. Representative results (means ± SEM) from at least two independent experiments are shown. In **A**–**D**, **F**, and **G**, significance was determined using a one-way ANOVA test; in **E**, significance for tumor sizes was determined using a two-way ANOVA test and for tumor weights using a one-way ANOVA test; and for immune cell infiltrates and activation markers in **C** and **F**, significance was determined using a two-tailed Mann–Whitney *U* test (#, $P > 0.05$; ##, $P > 0.01$). *, $P < 0.05$; **, $P < 0.01$; ***, $P < 0.001$; ****, $P < 0.0001$. ns, not significant.

CD69 cell-surface expression, and corrected the enhanced proliferation, as assessed by CTV dilution, and T-cell numbers (Fig. 5C and D). Therefore, the deletion of PTP1B promotes STAT5 signaling to facilitate the expansion and activation of T cells.

To determine whether heightened STAT5 signaling in PTP1B-deficient T cells may be responsible for enhanced antitumor activity, we implanted AT3-OVA tumor cells into the mammary fat pads of *Ptpn1*$^{fl/fl}$ versus *Lck*-Cre;*Ptpn1*$^{fl/fl}$ mice, as well as *Lck*-Cre;*Ptpn1*$^{fl/fl}$;*Stat5*$^{fl/+}$ mice, where the otherwise enhanced STAT5 signaling in T cells associated with PTP1B deficiency was corrected (Fig. 5E–G). We found that *Stat5* heterozygosity largely corrected the repression of syngeneic mammary tumor growth and the accumulation of PTP1B-deficient T cells in AT3-OVA mammary tumors (Fig. 5E and F). Moreover, *Stat5* heterozygosity completely corrected the enhanced cytotoxic activity of intratumoral CD8$^+$ T cells, as assessed by staining for IFNγ, TNF, and GZMB (Fig. 5G). Thus, PTP1B deletion enhances the proliferation, activation, cytotoxicity, and antitumor activity of CD8$^+$ T cells by promoting STAT5 signaling.

Targeting PTP1B Enhances Endogenous T-cell Antitumor Immunity

To interrogate PTP1B more directly as a potential therapeutic target for combatting cancer, we next determined whether the systemic inhibition of PTP1B with a small molecule might similarly enhance antitumor immunity. MSI-1436 is a specific allosteric inhibitor of PTP1B (19, 20) that has been reported to be safe and well tolerated in humans. Previous studies have shown that at 5 to 10 mg/kg, MSI-1436 administered intraperitoneally can repress the growth of HER2$^+$ breast cancer xenografts in immunocompromised mice (19). Accordingly, we administered C57BL/6 female mice bearing large (50 mm^2) AT3-OVA mammary tumors MSI-1436 at 2.5 to 10 mg/kg (intraperitoneally) every 3 days and monitored for effects on tumor growth and TILs. At 2.5 mg/kg, MSI-1436 had modest effects on tumor growth, but at 5 to 10 mg/kg, MSI-1436 markedly suppressed tumor growth (Fig. 6A; Supplementary Fig. S27A). At 5 mg/kg MSI-1436, the repression of tumor growth was accompanied by the infiltration of T cells, NK cells, and DCs that promote antitumor immunity, as well as immunosuppressive TAMs, MDSCs, and Tregs that were also seen in our genetic studies when PTP1B was deleted globally or within the hematopoietic compartment (Fig. 6B). The repression of tumor growth at 5 mg/kg MSI-1436 was accompanied by a significant increase in survival so that 33% of mice were alive 29 days after MSI-1436 treatment (Supplementary Fig. S27B). Importantly, the repression of tumor growth by MSI-1436 (5 mg/kg) could not be ascribed to the inhibition of PTP1B in tumor cells, as the deletion of PTP1B in AT3-OVA cells using CRISPR–Cas9 genome-editing in itself had no effect on tumor growth (Supplementary Fig. S28A and S28B). MSI-1436 administration (5 mg/kg) also suppressed the growth of B16F10-OVA melanoma and MC38-OVA colon cancer tumors injected into the flanks of C57BL/6 male mice (Fig. 6C and D). Therefore, the PTP1B inhibitor MSI-1436 can repress the growth of different syngeneic tumors in mice.

To determine the extent to which the repression of tumor growth by MSI-1436 might be attributable to the inhibition of PTP1B in T cells, we repeated these experiments in control (*Ptpn1*$^{fl/fl}$) versus T cell–specific PTP1B-deficient (*Lck*-Cre;*Ptpn1*$^{fl/fl}$) mice bearing AT3-OVA mammary tumors (Fig. 6E). The deletion of PTP1B in T cells or the administration of MSI-1436 (5 mg/kg) to control mice bearing AT3-OVA tumors similarly repressed tumor growth, but MSI-1436 had no additional effects on tumor growth in T cell–specific PTP1B-deficient mice (Fig. 6E). These results are consistent with the effects of MSI-1436 on tumor growth being mediated by the inhibition of PTP1B in T cells. In line with this, we found that the administration of MSI-1436 (5 mg/kg) was accompanied by increased naïve T cells in the spleen, as seen in *Lck*-Cre;*Ptpn1*$^{fl/fl}$ mice, as well as increased p-STAT5 and BCL2 in naïve, central memory, and effector/memory T cells in lymphoid organs (Supplementary Fig. S29A–S29C). As expected, the administration of MSI-1436 decreased body weight due to reductions in fat mass (Supplementary Fig. S30A and S30B). This is consistent with PTP1B's known role in attenuating hypothalamic leptin signaling (40) and the ability of MSI-1436 to decrease whole-body adiposity by repressing food intake (20). Importantly, MSI-1436 (5 mg/kg) decreased adiposity in both *Ptpn1*$^{fl/fl}$ and *Lck*-Cre;*Ptpn1*$^{fl/fl}$ mice (Supplementary Fig. S30B), suggesting that the repression of tumor growth was independent of the effects on adiposity. Interestingly, although MSI-1436 treatment and the genetic deletion of PTP1B in T cells similarly repressed tumor growth, MSI-1436 treatment resulted in a greater number of effector/memory T cells within tumors (Supplementary Fig. S31), indicating that MSI-1436 might also elicit T cell–independent effects to affect T-cell recruitment and/or activation.

Finally, we determined whether the response to MSI-1436 might be enhanced further by the concomitant blockade of the cell-surface immune checkpoint molecule PD-1. Female mice bearing large AT3-OVA mammary tumors were treated with MSI-1436 (5–10 mg/kg) alone every third day, anti–PD-1 alone every fourth day, or MSI-1436 plus anti–PD-1,

Figure 6. The inhibition of PTP1B in T cells promotes antitumor immunity. **A** and **B,** AT3-OVA mammary tumor cells were implanted into the fourth inguinal mammary fat pads of C57BL/6 mice. Mice were treated with MSI-1436 (5 mg/kg, i.p.) or saline on days 14, 17, 20, 23, 26, and 29 after tumor cell implantation. Tumor growth was monitored (**A**), and TILs including CD4$^+$, CD8$^+$ T cells, CD19$^+$ B cells, NK1.1$^+$TCRβ$^-$ NK cells, CD11c$^+$ DCs, CD4$^+$CD25$^+$FoxP3$^+$ Tregs, CD11b$^+$F4/80^{hi}Ly6C$^-$Ly6G$^-$ TAMs, granulocytic CD11b$^+$F4/80$^{hi/lo}$Ly6C^{int}Ly6G$^+$ MDSCs (gMDSCs), and monocytic CD11b$^+$F4/80$^{hi/lo}$Ly6C$^+$Ly6G$^-$ MDSCs (mMDSCs) were analyzed by flow cytometry (**B**). B16F10-OVA (**C**) or MC38-OVA (**D**) tumor cells were xenografted into the flanks of C57BL/6 male mice. Mice were treated every 3 days with saline or MSI-1436 (5 mg/kg, i.p.) once tumors (40–50 mm^2) were established (days 7, 10, and 13 for B16F10-OVA tumors or days 7, 10, 13, 16, 19, and 22 for MC38-OVA tumors), and tumor growth monitored. **E,** AT3-OVA tumor cells were implanted into the fourth inguinal mammary fat pads of *Ptpn1*$^{fl/fl}$ versus *Lck*-Cre;*Ptpn1*$^{fl/fl}$ mice. After tumors were established, mice were treated every 3 days with saline or MSI-1436 (5 mg/kg, i.p. on days 14, 17, 20, 23, and 26) and tumor growth monitored. **F,** AT3-OVA tumor cells were implanted into the fourth inguinal mammary fat pads of C57BL/6 mice. Mice were treated with MSI-1436 (10 mg/kg, i.p. on days 13, 16, 19, 22, and 25) and either anti–PD-1 (αPD-1) or isotype control (200 μg, i.p. in each case on days 13, 17, 21, and 24) alone or MSI-1436 plus αPD-1. Tumor growth was monitored, and tumor weights were determined. Representative results (means ± SEM) from at least two independent experiments are shown. Significance for tumor sizes in **A** and **C**–**F** was determined using a two-way ANOVA test and for TILs in **B** using a two-tailed Mann–Whitney *U* test. *, $P < 0.05$; **, $P < 0.01$; ***, $P < 0.001$.

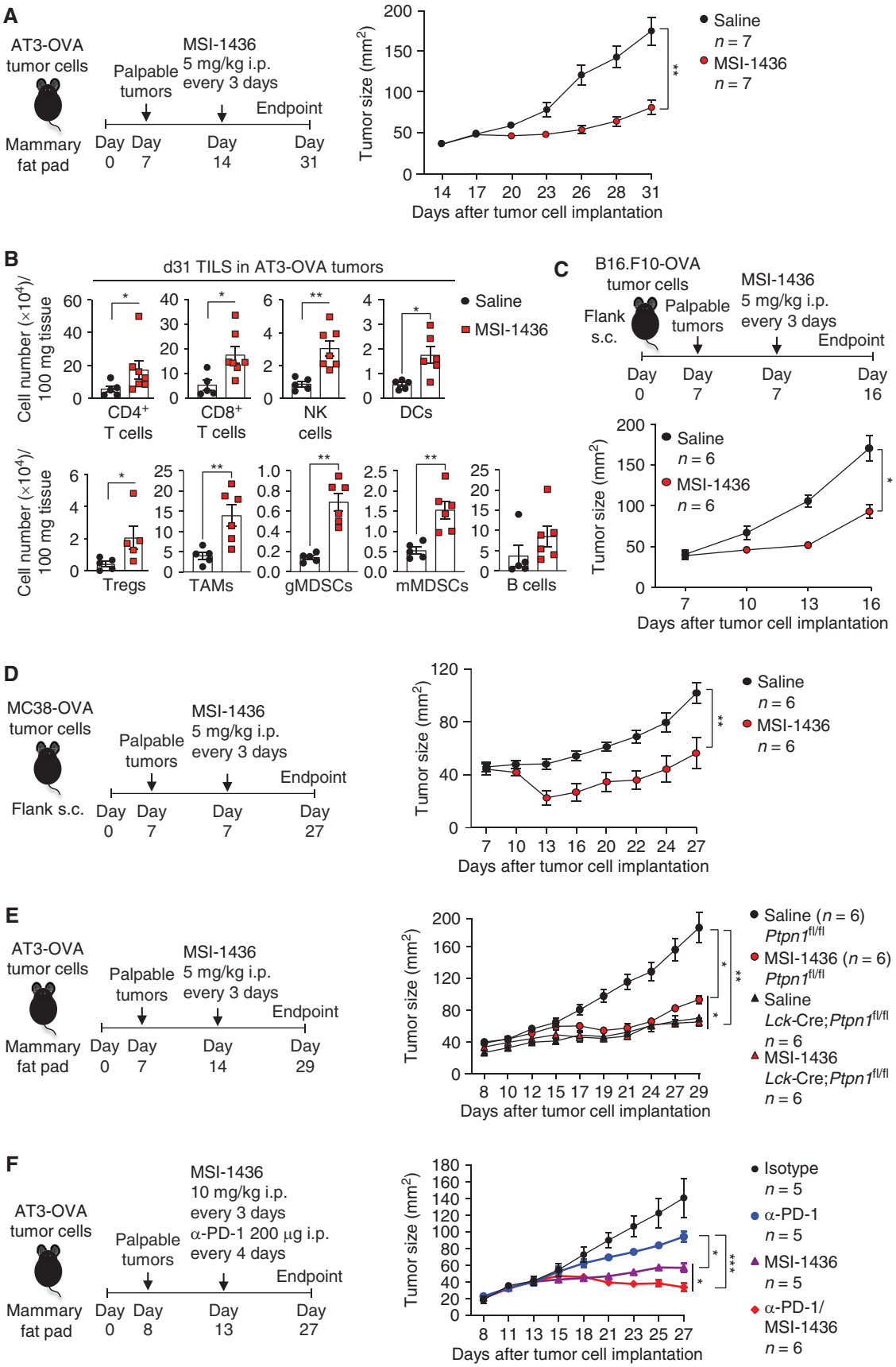
A
AT3-OVA tumor cells
Mammary fat pad
Palpable tumors
MSI-1436 5 mg/kg i.p. every 3 days
Endpoint
Day 0
Day 7
Day 14
Day 31
Tumor size (mm²)
Days after tumor cell implantation
Saline n = 7
MSI-1436 n = 7
B
d31 TILS in AT3-OVA tumors
Cell number (×10⁴)/100 mg tissue
CD4⁺ T cells
CD8⁺ T cells
NK cells
DCs
Tregs
TAMs
gMDSCs
mMDSCs
B cells
Saline
MSI-1436
C
B16.F10-OVA tumor cells
Flank s.c.
Palpable tumors
MSI-1436 5 mg/kg i.p. every 3 days
Endpoint
Day 0
Day 7
Day 7
Day 16
Saline n = 6
MSI-1436 n = 6
D
MC38-OVA tumor cells
Flank s.c.
Palpable tumors
MSI-1436 5 mg/kg i.p. every 3 days
Endpoint
Day 0
Day 7
Day 7
Day 27
Saline n = 6
MSI-1436 n = 6
E
AT3-OVA tumor cells
Mammary fat pad
Palpable tumors
MSI-1436 5 mg/kg i.p. every 3 days
Endpoint
Day 0
Day 7
Day 14
Day 29
Saline (n = 6) Ptpn1fl/fl
MSI-1436 (n = 6) Ptpn1fl/fl
Saline Lck-Cre;Ptpn1fl/fl n = 6
MSI-1436 Lck-Cre;Ptpn1fl/fl n = 6
F
AT3-OVA tumor cells
Mammary fat pad
Palpable tumors
MSI-1436 10 mg/kg i.p. every 3 days
α-PD-1 200 μg i.p. every 4 days
Endpoint
Day 0
Day 8
Day 13
Day 27
Isotype n = 5
α-PD-1 n = 5
MSI-1436 n = 5
α-PD-1/ MSI-1436 n = 6

and tumor growth was assessed (Fig. 6F; Supplementary Fig. S32A and S32B). At 5 mg/kg, MSI-1436 was just as effective and at 10 mg/kg more effective at repressing tumor growth than anti–PD-1 alone, but the addition of anti–PD-1 in either case further enhanced the repression of tumor growth (Fig. 6F; Supplementary Fig. S32A). Importantly, the combined treatment of MSI-1436 plus anti–PD-1 had no additional impact on tumor effector/memory T-cell numbers, but decreased the proportion of PD-1^{+}Tim3^{hi} CD8^{+} T cells, consistent with the alleviation of T-cell exhaustion (Supplementary Fig. S32B). These findings demonstrate that PTP1B can enhance T cell–mediated antitumor immunity, and this effect can be enhanced further by targeting the PD-1 checkpoint.

Targeting PTP1B Enhances CAR T-cell Antitumor Immunity

CAR T-cell therapy has emerged as an exciting immunotherapy approach for nonimmunogenic cancers, as it does not rely on endogenous antitumor immunity (41). Given the marked improvements in T cell–mediated antitumor immunity resulting from the deletion or inhibition of PTP1B, we examined whether targeting PTP1B might also enhance the efficacy of adoptively transferred CAR T cells in a solid tumor setting. To this end, we assessed the impact of deleting or inhibiting PTP1B on the activity of second-generation CAR T cells targeting the human ortholog of murine ErbB2/Neu, HER2 (42). The deletion of PTP1B did not affect the generation of CAR T cells *in vitro* (Supplementary Fig. S33A), but enhanced their antigen-specific activation (Supplementary Fig. S33B and S33C) and their capacity to kill HER2-expressing 24JK sarcoma cells (HER2-24JK) specifically *in vitro* (Supplementary Fig. S33D). To assess the impact of PTP1B deficiency on the therapeutic efficacy of CAR T cells in *vivo*, we adoptively transferred *Ptpn1*$^{fl/fl}$ or *Lck*-Cre;*Ptpn1*$^{fl/fl}$ αHER2 CAR T cells into sublethally irradiated hosts bearing established (25–30 mm^2) orthotopic tumors arising from the injection of HER2-expressing E0771 (HER2-E0771) mammary tumor cells (Fig. 7A–D); E0771 mammary tumors resemble human triple-negative breast cancer, as they are estrogen receptor–, progesterone receptor–, and ErbB2-negative, basal-like, and mutant for *Trp53* and are characterized by a robust immunosuppressive tumor microenvironment (11, 43). HER2-E0771 cells were grafted into nulliparous human HER2 TG female mice, where HER2 expression is driven by the whey acidic protein (WAP) promoter, which induces expression in the lactating mammary gland and the cerebellum (44); this ensures that human HER2-expressing orthotopic tumors are regarded as self, so that host antitumor immunity is repressed. Strikingly, whereas the adoptive transfer of *Ptpn1*$^{fl/fl}$ control αHER2 CAR T cells had little, if any effect on tumor growth, PTP1B-deficient αHER2 CAR T cells markedly repressed tumor growth (Fig. 7A). This was accompanied by a significant increase in the number of PTP1B-deficient CAR T cells in the tumor, but not in the spleen (Fig. 7C), consistent with PTP1B deficiency driving antigen-induced CAR T-cell expansion. Moreover, intratumoral PTP1B-deficient CAR T cells exhibited enhanced cytotoxicity, as reflected by the increased expression of TNF, IFNγ, and GZMB (Fig. 7D). The enhanced CAR T-cell activation/cytotoxicity and repression of tumor growth were accompanied by a significantly enhanced survival of tumor-bearing mice (Fig. 7B). Importantly, the adoptive transfer of PTP1B-deficient CAR T cells did not promote systemic inflammation (Supplementary Fig. S34A–S34F), as assessed by monitoring for lymphocytic infiltrates in nonlymphoid tissues, including the contralateral mammary glands, lungs, and livers (Supplementary Fig. S34B), or for circulating IL6, IFNγ, and TNF (Supplementary Fig. S34C). Moreover, PTP1B-deficient CAR T cells did promote overt morbidity, as assessed by gross appearance or by measuring food intake, ambulatory activity, voluntary wheel running, and energy expenditure (Supplementary Fig. S34D). Furthermore, although the WAP promoter in nulliparous HER2 TG mice drives HER2 expression in the cerebellum (11, 44), there were no overt signs of cerebellar tissue damage (Supplementary Fig. S34E), and the cerebellar control of neuromotor function, as assessed in rotarod tests, was not affected (Supplementary Fig. S34F).

To determine whether the inhibition of PTP1B might similarly enhance CAR T-cell efficacy, we administered tumor (HER2-E0771)-bearing HER2 TG mice that had been sublethally irradiated and then left untreated or treated with control (*Ptpn1*$^{fl/fl}$) or PTP1B-defcient (*Ptpn1*$^{fl/fl}$ or *Lck*-Cre;*Ptpn1*$^{fl/fl}$) αHER2 CAR T cells with MSI-1436 (5 mg/kg) every 3 days (Fig. 7E–G). In mice not treated with CAR T cells, the inhibitor had little effect, probably because the sublethal irradiation depletes T cells (Supplementary Fig. S35). By contrast, the inhibitor markedly enhanced the ability of αHER2 CAR T cells to repress tumor growth, so that they were just as effective as those treated with PTP1B-deficient CAR T cells (Fig. 7E and F). The repression of tumor growth in mice treated with MSI-1436 was accompanied by a significant increase in the number of CAR T cells in the tumor (Fig. 7G). Taken together, our results demonstrate that targeting PTP1B can not only enhance the antitumor activity of endogenous T cells and synergize with the blockade of cell-surface checkpoints such as PD-1, but also enhance the efficacy of adoptively transferred CAR T cells.

Figure 7. Targeting PTP1B enhances CAR T-cell cytotoxicity and efficacy. **A–D,** HER2-E0771 mammary tumor cells were injected into the fourth inguinal mammary fat pads of female HER2 TG mice. Seven days after tumor injection, HER2 TG mice received total body irradiation (4 Gy) followed by the adoptive transfer of 2×10^7 HER2 CAR T cells generated from *Ptpn1*$^{fl/fl}$ or *Lck*-Cre;*Ptpn1*$^{fl/fl}$ splenocytes. Tumor growth (**A**) and survival (**B**) were monitored, and CD45^{+}CD8^{+}mCherry^{+} CAR T-cell infiltrates (**C**) were determined by flow cytometry at day 8 after adoptive transfer. **D,** Tumor-infiltrating HER2 CAR T cells were stimulated with phorbol 12-myristate 13-acetate/ionomycin in the presence of Golgi Stop/Plug and stained for intracellular IFNγ and TNF. Intracellular GZMB was detected in unstimulated CD8^{+} HER2 CAR T-cell tumor infiltrates. **E–G,** Tumor-bearing HER2 TG mice were treated every 3 days with saline or MSI-1436 (5 mg/kg, i.p.) on days 1, 4, 7, 10, 13, 16, and 19 after adoptive HER2 CAR T-cell transfer, and tumor growth was monitored and tumor weights were determined (**F**). **G,** CD8^{+}mCherry^{+} HER2 CAR T-cell infiltrates were determined by flow cytometry at day 23 after adoptive transfer. Representative results (means ± SEM) from at least two independent experiments are shown. Significance for tumor sizes in **A** and **E** was determined using two-way ANOVA test. Significance for TILs and intracellular IFNγ, TNF, and GRZB levels in **C** and **D** was determined using a two-tailed Mann–Whitney *U* test; significance for tumor weights in **F** and TILs in **G** was determined using a one-way ANOVA test or two-tailed Mann–Whitney *U* test (*, $P < 0.05$) and in **B** using a log-rank (Mantel–Cox) test. *, $P < 0.05$; **, $P < 0.01$; ***, $P < 0.001$; ****, $P < 0.0001$.

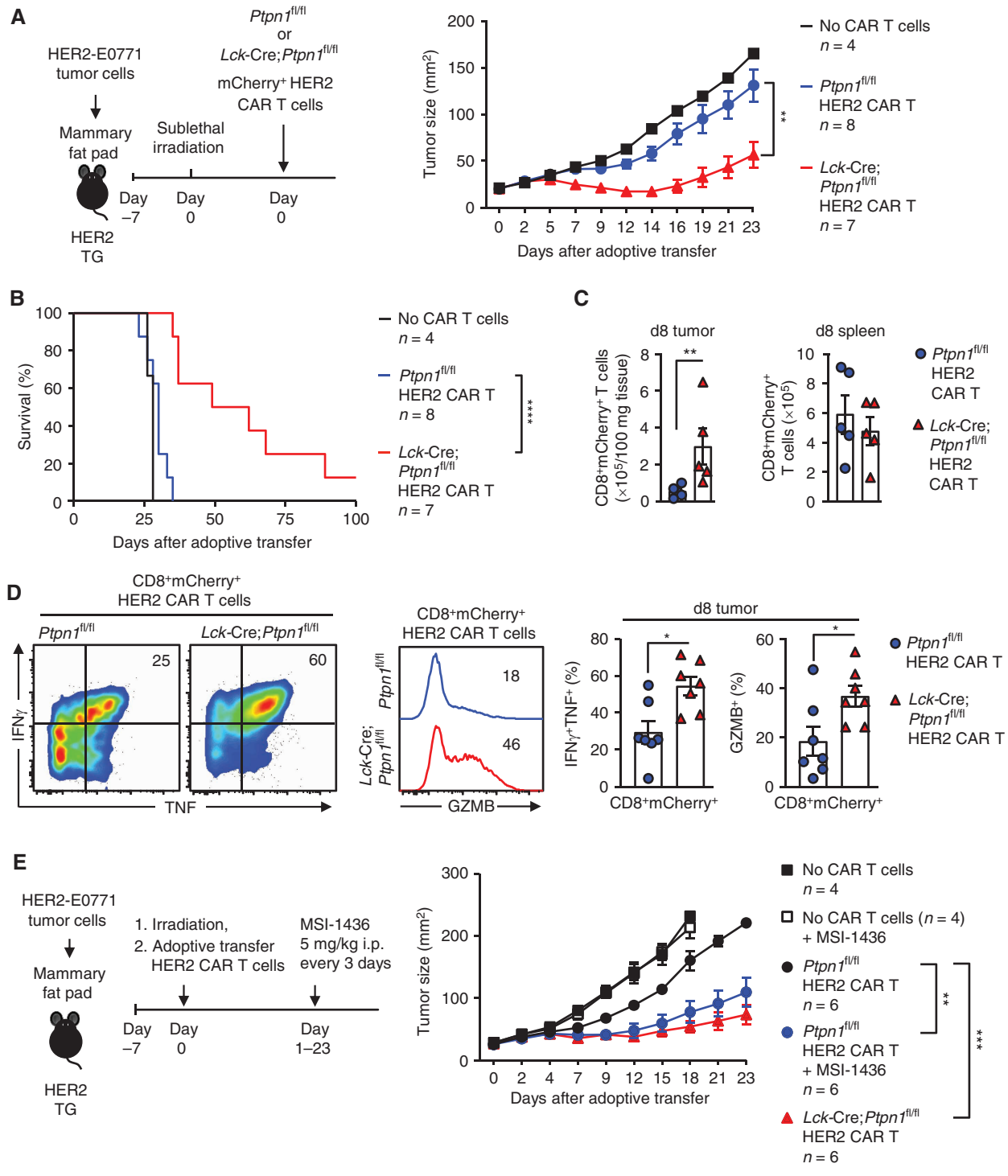
A
HER2-E0771 tumor cells
Mammary fat pad
HER2 TG
Ptpn1fl/fl or Lck-Cre;Ptpn1fl/fl mCherry+ HER2 CAR T cells
Sublethal irradiation
Day −7
Day 0
Day 0
Tumor size (mm2)
Days after adoptive transfer
No CAR T cells n = 4
Ptpn1fl/fl HER2 CAR T n = 8
Lck-Cre; Ptpn1fl/fl HER2 CAR T n = 7
B
Survival (%)
Days after adoptive transfer
C
d8 tumor
d8 spleen
CD8+mCherry+ T cells (×10^5/100 mg tissue)
CD8+mCherry+ T cells (×10^5)
D
CD8+mCherry+ HER2 CAR T cells
IFNγ
TNF
GZMB
IFNγ+TNF+ (%)
GZMB+ (%)
E
HER2-E0771 tumor cells
1. Irradiation, 2. Adoptive transfer HER2 CAR T cells
MSI-1436 5 mg/kg i.p. every 3 days
Day −7
Day 0
Day 1–23
No CAR T cells (n = 4) + MSI-1436
Ptpn1fl/fl HER2 CAR T + MSI-1436 n = 6
F
d23 tumors
Weight (mg × 10^2)
G
d23 tumor
d23 spleen
CD8+mCherry+ T cells (×10^3/100 mg tissue)

DISCUSSION

Our increasing understanding of how cancer evades the immune system has been instrumental in designing therapies that induce or even reinstate the patient's immune response to tumor cells. The clinical successes of checkpoint inhibitors directed against PD-1 and CTLA4 in this regard stem from decades of research focused on understanding T-cell biology and mechanisms governing T-cell tolerance. In this study, we show for the first time that PTP1B is of fundamental importance in coordinating JAK/STAT5 signaling in T cells and thereby the activation, expansion, and cytotoxic activity of T cells. We demonstrate that the expression of PTP1B is increased in effector/memory CD8$^+$ T cells that infiltrate tumors in mice, or in effector and exhausted CD8$^+$ T cells that infiltrate melanomas in humans. We demonstrate that the induction of PTP1B in intratumoral CD8$^+$ T cells can limit T-cell expansion and cytotoxicity, and thereby facilitate tumor growth. Importantly, we report that the deletion or inhibition of PTP1B can overcome such inhibitory constraints to enhance the antitumor activity of T cells, and the efficacy of adoptively transferred CAR T cells, without promoting autoimmunity and systemic inflammation.

Our results indicate that the induction of PTP1B in intratumoral T cells in mice occurs as a consequence of the tumor microenvironment, rather than T-cell differentiation or activation *per se*, because PTP1B was elevated similarly in both endogenous and adoptively transferred (OT-I) effector/memory CD8$^+$ T cells within tumors when compared with the corresponding T cells in the spleen. Although different aspects of the tumor microenvironment may be responsible for the induction of PTP1B in infiltrating T cells, inflammation is likely to be an important contributing factor. It is well established that inflammation can facilitate malignant growth by both directly promoting the growth of tumor cells and by shaping the immune response. Previous studies have shown that PTP1B expression can be induced by the inflammatory cytokine TNF and via the recruitment of NFκB to the *PTPN1* promoter (45). TNF acts by binding to TNFR1, which is expressed widely, and TNFR2, which is expressed on immune cells, including activated T cells. In tumors, TNF may limit T-cell responses, because the blockade of TNF–TNFR1 signaling can increase tumor-specific CD8$^+$ T-cell responses (46), whereas mAbs targeting TNFR2 enhance T cell–mediated antitumor immunity (47). It would be interesting to determine the extent to which TNF might be responsible for the induction of PTP1B in intratumoral T cells and whether the benefits of TNFR blockade on antitumor immunity (46, 47) might be reliant on the repression of PTP1B in T cells. Irrespective, we found that the deletion or inhibition of PTP1B enhanced the antigen-induced expansion and activation of naïve T cells and the cytotoxicity of effector CD8$^+$ T cells to inhibit the growth of syngeneic tumors. Importantly, correcting the increased PTP1B levels in intratumoral T cells in *Lck*-Cre;*Ptpn1*$^{fl/+}$ heterozygous mice was sufficient to facilitate the accumulation of effector T cells within tumors and repress tumor growth. As such, our studies are consistent with PTP1B acting as an intracellular checkpoint whose inhibition can enhance CD8$^+$ T cell–mediated antitumor immunity to repress tumor growth.

Our results show that the ability of PTP1B-deficient T cells to repress tumor growth in mice is reliant on the promotion of JAK/STAT5 signaling. Early studies established that PTP1B could directly dephosphorylate and inactivate JAK2 and TYK2 to attenuate cytokine-induced JAK/STAT signaling; there is also evidence that PTP1B can directly dephosphorylate some STAT family members (29, 30, 48). Consistent with this, basal STAT5 Y694 phosphorylation and cytokine-induced TYK2 Y1054/Y1055 and STAT5 Y694 phosphorylation were enhanced by the deletion of PTP1B. This was attributable to both increased JAK activation and prolonged STAT5 Y694 phosphorylation, consistent with PTP1B acting directly on both JAKs and STAT5. The enhanced STAT5 signaling was evident in both naïve and memory CD4$^+$ and CD8$^+$ T cells and was accompanied by the induction of STAT5 transcriptional targets, including T-bet and Eomes, which are important for CD8$^+$ T-cell cytotoxicity and antitumor immunity (49); BCL2, which promotes cell survival; and CD25 (IL2R α chain), which together with IL2Rβ and the γc chain constitute the high-affinity receptor for IL2 (28). PTP1B deficiency also enhanced cytokine-induced STAT5 signaling, especially IL2-induced STAT5 signaling in CD8$^+$ effector T cells, where IL2 promotes cytotoxicity by increasing the expression of IFNγ, TNF, and GZMB (28). The heightened basal and cytokine-induced STAT5 signaling were accompanied by an increase in overall thymocyte and T-cell numbers, including thymic and peripheral CD4$^+$ Tregs whose generation and maintenance are reliant on IL2 (28), as well as heightened TCR-induced naïve CD4$^+$ and CD8$^+$ T-cell expansion and activation and effector CD8$^+$ T-cell cytotoxicity and antitumor immunity. As in murine T cells, the deletion of PTP1B also increased STAT5 signaling and the TCR-instigated expansion and activation of human T cells. The enhanced T-cell responses and superior tumor control in mice were attenuated when the heightened STAT5 signaling was corrected by crossing *Lck*-Cre;*Ptpn1*$^{fl/fl}$ mice onto a *Stat5*$^{fl/+}$ background. Although we cannot exclude that PTP1B might also influence other tyrosine phosphorylation–dependent signaling pathways, our studies indicate that its effects on STAT5 signaling are nonetheless instrumental in its capacity to act as an intracellular checkpoint and influence tumor growth.

We demonstrated that the effects of PTP1B deletion on the T cell–mediated repression of tumor growth phenocopied those in mice in which PTP1B was deleted globally or throughout the hematopoietic compartment. Moreover, we found that the inhibition of PTP1B with MSI-1436 repressed tumor growth by targeting PTP1B in T cells, as its administration had no additional impact in *Lck*-Cre;*Ptpn1*$^{fl/fl}$ mice. However, it is possible that in some circumstances, the inhibition of PTP1B in tumor cells, or other components of the immune system, might also contribute to the repression of tumor growth. PTP1B is required for the growth and metastasis of HER2/ErbB2-expressing tumors (19, 22, 23). As such, it would be interesting to determine whether the combined targeting of PTP1B in ErbB2-driven mammary tumors and T cells might yield synergistic outcomes. Furthermore, previous studies have shown that the heterozygous deletion of PTP1B enhances DC maturation and immunogenicity and represses the growth of B-cell lymphomas (25). Specifically, Eμ-myc–driven B-cell lymphomas

are attenuated in *Ptpn1*$^{+/-}$ mice, and this is accompanied by enhanced DC maturation and immunogenicity, as well as repressed Treg and MDSC recruitment (25). By contrast, DCs are more tolerogenic in *Ptpn1*$^{-/-}$ mice (26). We found that repression of syngeneic tumor growth, resulting from the global or hematopoietic-specific deletion of PTP1B, or the systemic inhibition of PTP1B, was accompanied by the recruitment of not only T cells and NK cells, but also DCs, Tregs, and MDSCs. Although we did not assess DC maturation, any potential effect on DCs appeared to be of limited importance, as the repression of tumor growth was phenocopied in *Lck*-Cre;*Ptpn1*$^{fl/fl}$ mice, whereas MSI-1436 neither enhanced nor antagonized the repression of tumor growth in *Lck*-Cre;*Ptpn1*$^{fl/fl}$ mice. Nonetheless, MSI-1436 treatment increased intratumoral T cells even in *Lck*-Cre;*Ptpn1*$^{fl/fl}$ mice, and this could have occurred as a consequence of PTP1B inhibition in DCs to drive licensing and T-cell expansion. Therefore, depending on the tumor, there may be additional tumor cell–autonomous and non–cell autonomous benefits of systemically targeting PTP1B in cancer.

Our studies indicate that inhibition of PTP1B can be more effective at suppressing tumor growth than blockade of PD-1. Moreover, we found that combining PTP1B inhibition with PD-1 checkpoint blockade led to a greater tumor repression than either treatment alone. These results suggest that PTP1B acts independently of PD-1 inhibitory signaling. Whereas PD-1 functions to attenuate TCR and potentially coreceptor signaling (6), we demonstrate that PTP1B functions to attenuate cytokine signaling, including that mediated by IL2. Durable clinical responses with PD-1 monotherapy are only evident in a subset of patients, with most developing transient responses or no responses at all (1, 3). Some studies suggest that inhibitory PD-1 signaling in T cells and CAR T cells can be overcome by promoting IL2 responses and signaling via STAT5 (50, 51). Therefore, targeting PTP1B may afford a means for promoting IL2/STAT5 signaling and alleviating PD-1 inhibitory signaling to extend the utility and/or durability of PD-1 checkpoint blockade. In our studies, we found that the combined targeting of PTP1B and PD-1 decreased T-cell exhaustion, but the precise mechanisms involved remain to be determined.

Beyond the potential to enhance endogenous antitumor immunity and the response to anti–PD-1 therapy, our studies also establish the therapeutic potential of targeting PTP1B in adoptive cellular immunotherapy. In particular, we demonstrated that the genetic or pharmacologic targeting of PTP1B in CAR T cells enhanced the activation and therapeutic efficacy of CAR T cells *in vivo*. To date, CAR T cells have been highly effective in combating hematologic malignancies. In particular, CAR T cells targeting the B-cell lineage–restricted protein CD19 have transformed the treatment of B-cell acute lymphoblastic leukemia (41). However, CAR T cells have been largely ineffective against solid tumors (41). Herein we demonstrate that targeting PTP1B can enhance the efficacy of adoptively transferred CAR T cells and repress the growth of highly aggressive and otherwise highly immunosuppressive E0771 mammary tumors to significantly extend survival. Notably, the inhibition of PTP1B with MSI-1436 was just as effective at enhancing the efficacy of CAR T cells as the genetic deletion of PTP1B. In these studies, the administration of MSI-1436 had no impact on endogenous antitumor immunity, because the mice were first lymphodepleted by irradiation to allow for the effective expansion of adoptively transferred CAR T cells. Although lymphodepletion typically is also common in the clinic, an added potential benefit of systemically targeting PTP1B with MSI-1436 might be the alleviation of inhibitory constraints imposed on endogenous tumor-resident T cells, which might serve to prevent the emergence of antigen loss tumor variants during CAR T-cell therapy (52). Similar outcomes have been sought when CAR T-cell therapies have been combined with PD-1 blockade or oncolytic vaccines (43, 52, 53). Although further studies are required to explore such possibilities, targeting PTP1B with specific inhibitors stands to transform CAR T-cell therapy and readily extend the utility of CAR T cells to the effective therapy of recalcitrant solid tumors.

In summary, our studies identify PTP1B as an integral negative regulator of T-cell function and an intracellular T-cell checkpoint that limits the antitumor immunity of tumor-infiltrated CD8$^+$ T cells. We demonstrate that the inhibition of PTP1B in cancer can enhance endogenous T cell–mediated antitumor immunity, akin to that seen by targeting the cell-surface checkpoint PD-1 that has revolutionized cancer therapy. Furthermore, the inhibition or genetic deletion of PTP1B can overcome a major hurdle that has thus far limited the effectiveness of CAR T cells against solid tumors. Our studies demonstrate that targeting PTP1B with inhibitors such as MSI-1436 may provide an alternative therapeutic strategy for enhancing T cell–mediated antitumor immunity to combat cancer.

METHODS

Materials

For T-cell stimulations, CD3ε (BD Biosciences, catalog no. 553058, RRID:AB_394591) and CD28 (BD Biosciences, catalog no. 557393, RRID:AB_396676) antibodies were purchased from BD Biosciences. p-(Y418) SFK (Thermo Fisher Scientific, catalog no. 14–9034–82) was purchased from Invitrogen. Antibodies to p-(1054/Y1055) TYK2 (catalog no. 9321, RRID:AB_2303972), p-(Y493) ZAP70 (catalog no. 2704, RRID:AB_2217457), p-ERK1/2 (catalog no. 4376, RRID:AB_331772), LCK (catalog no. 2752, RRID:AB_2234649), ZAP-70 (catalog no. 3165, RRID:AB_2218656), ERK1/2 (catalog no. 9102, RRID:AB_330744), and p-(Y694) STAT5 (D47E7) XP (catalog no. 4322, RRID:AB_10544692) were from Cell Signaling Technology; the pTyr (4G10) antibody was from the Monash Antibodies Technologies Facility; anti-actin (catalog no. MA5–11866, RRID:AB_10985365) and anti-vinculin (catalog no. MA1–25018, RRID:AB_795706) were from Thermo Fisher Scientific; rabbit monoclonal PTP1B (catalog no. ab244207, RRID:AB_2877148) antibody for flow cytometry was from Abcam; and goat polyclonal PTP1B (catalog no. AF3954, RRID:AB_2174947) antibody for immunoblotting was from R&D Systems. Recombinant human IL2, murine IL7, and human IL15 used for T-cell stimulations or the generation of CAR T cells were purchased from PeproTech. *InVivo*MAb anti-mouse PD-1 (catalog no. BE0146, RRID:AB_10949053) and *InVivo*MAb rat IgG2a isotype control (catalog no. BE0251, RRID:AB_2687732) were purchased from Bio X Cell. MSI-1436 was provided by DepYmed, Inc., and RetroNectin was purchased from Takara, ruxolitinib from Selleckchem, and Dnase I from Sigma-Aldrich. The mouse antinuclear antibody Igs (total IgA+G+M) ELISA Kit was from Alpha Diagnostic; the Transaminase II Kit was from Wako Pure Chemicals; and the BD Pharmingen APC BrdU

Flow Kit and the PE Annexin V Apoptosis Detection Kit II were from BD Biosciences. FBS was purchased from Thermo Scientific; RPMI 1640, DMEM, MEM, 4-(2-hydroxyethyl)-1-piperazineethanesulfonic acid (HEPES), nonessential amino acids, penicillin/streptomycin, and sodium pyruvate were from Invitrogen; and collagenase type IV was from Worthington Biochemicals.

Mice

Mice were maintained on a 12-hour light–dark cycle in a temperature-controlled high-barrier facility with free access to food and water. Six- to 12-week-old female B6.SJL-*Ptprc*^{a}*Pepc*^{b}/BoyJ (Ly5.1) and human HER2 TG–recipient mice and 6- to 10-week-old female donor mice were used for adoptive transfers. Age- and sex-matched littermates were used in all experiments; unless otherwise indicated, female donor mice were used for all in *vivo* experiments, whereas mice of the same sex were used for *ex vivo* experiments. *Ptpn1*$^{fl/fl}$ (C57BL/6; RRID:MMRRC_032243-JAX), *Lck*-Cre (C57BL/6; RRID:IMSR_JAX:006889), OT-I (RRID:IMSR_JAX:003831), *Stat5*$^{fl/fl}$ (C57BL/6; OT-I RRID:MMRRC_032053-JAX), *Ptpn1*$^{-/-}$ (C57BL/6; RRID:MMRRC_032240-JAX), and human HER2 TG (C57BL/6) mice have been described previously (7, 11, 17, 40). *Lck*-Cre mice were mated with *Ptpn1*$^{fl/fl}$ mice and thereon interbred to generate *Lck*-Cre;*Ptpn1*$^{fl/fl}$ mice that were subsequently mated with either OT-I or *Stat5*$^{fl/fl}$ mice to generate OT-I;*Lck*-Cre;*Ptpn1*$^{fl/fl}$ or *Lck*-Cre;*Ptpn1*$^{fl/fl}$;*Stat5*$^{fl/+}$ mice, respectively. Ly5.1 (RRID:IMSR_JAX:002014) and C57BL/6J (RRID:IMSR_JAX:000664) mice were purchased from the Walter and Eliza Hall Institute of Medical Research (WEHI) Animal Facility or from the Animal Resource Centre (Perth, Australia).

Mouse Behavioral Assessments

Food intake, ambulatory activity, wheel running, and energy expenditure were assessed over 48 hours after 24 hours acclimation using a Promethion Metabolic Screening System (Sable Systems International) fitted with indirect open circuit calorimetry, running wheels, and food consumption and activity monitors.

Neuromotor function was assessed with rotarod tests. Mice were trained once per day for 4 days on a rotating rod with a lane width of 5 cm (Ugo Basile Rota-Rod 476000) spinning at 4 rpm for 5 minutes. After training, mice were subjected to an incremental protocol, where the speed was increased over 480 seconds from 4 to 60 rpm. All animals were subjected to four independent trials separated by 1 hour, and the latency to fall (length of time that the mice remained on the rod) was recorded and analyzed.

Cell Lines

The C57BL/6 mouse mammary tumor cell line AT3 (Millipore, catalog no. SCC178, RRID:CVCL_VR89), the mouse melanoma cell line B16F10 (ATCC, catalog no. CRL-6475, RRID:CVCL_0159), and the mouse colon carcinoma cell line MC38 (RRID:CVCL_B288) and those engineered to express chicken OVA (AT3-OVA, B16F10-OVA, and MC38-OVA) have been described previously (11, 54). The C57BL/6 mouse breast carcinoma cell line E0771 (ATCC, catalog no. CRL-3461, RRID:CVCL_GR23), the C57BL/6 mouse sarcoma cell line 24JK, and those engineered to express truncated human HER2 (HER2-E0771) have been described previously (11). All tumor cell lines were maintained in high-glucose DMEM supplemented with 10% (v/v) FBS, L-glutamine (2 mmol/L), penicillin (100 U/mL)/streptomycin (100 μg/mL), and HEPES (10 mmol/L). All tumor cell lines were provided by the Peter MacCallum Cancer Centre and authenticated for their antigen/marker expression by flow cytometry. 24JK, HER2-24JK, and HER2-E0771 cell lines were received in March 2017. AT3 and AT3-OVA cell lines were received in August 2017. B16F10-OVA and MC38-OVA cell lines were received in April 2020. The B16F10 and MC38 cell lines were received in April 2021. Cells were routinely tested for *Mycoplasma* contamination by PCR and maintained in culture for less than 4 weeks. All tumor cell lines used came from early frozen batches, between passages two and five after receipt.

Flow Cytometry

Single-cell suspensions from thymus, spleen, and lymph nodes were obtained as described previously (7). For the detection of intracellular cytokines, GZMB or PTP1B, T cells were fixed and permeabilized with the BD Cytofix/Cytoperm Kit according to the manufacturer's instructions. Briefly, T cells were surface stained with fluorophore-conjugated antibodies and then fixed and permeabilized on ice for 20 minutes. Cells were stained intracellularly with the PTP1B monoclonal rabbit antibody (1/200 for 45 minutes at room temperature), which was detected by the secondary antibody against rabbit IgG (H+L) F(ab′)$_2$ fragment conjugated to Alexa Fluor 647 (Jackson ImmunoResearch Laboratories, catalog no. 111–606–003, RRID:AB_2338079; 30 minutes, room temperature). Alternatively, fixed and permeabilized T cells were stained for IFNγ, TNF, and GZMB for 45 minutes at room temperature. For the detection of intracellular FoxP3, Eomes, and T-bet, the Foxp3/Transcription Factor Staining Buffer Set (eBioscience) was used according to the manufacturer's instructions. Briefly, T cells were fixed and permeabilized for 1 hour on ice, and intracellular staining was performed at room temperature for 45 minutes. For the detection of serum cytokines, the BD CBA Mouse Inflammation Kit was used according to the manufacturer's instructions. The BD Pharmingen BrdU Flow Kit from BD Biosciences was used to detect intracellular BrdU in T cells according to the manufacturer's instructions. The PE Annexin V Apoptosis Detection Kit II from BD Biosciences was used to detect apoptotic T cells according to the manufacturer's instructions.

Cells were stained with the specified antibodies on ice for 30 minutes and analyzed using an LSRII (BD Biosciences), Fortessa (BD Biosciences), Symphony (BD Biosciences), or CyAn ADP (Beckman Coulter). For FACS, cells were stained for 30 minutes on ice and purified using either a BD Influx cell sorter or the BD FACSAria II, BD FACSAria Fusion 3, or BD FACSAria Fusion 5 instruments. Data were analyzed using FlowJo10 (Tree Star Inc.) software. For cell quantification, a known number of Calibrite Beads (BD Biosciences) or Nile Red Beads (Prositech) or Flow-Count Fluorospheres (Beckman Coulter) were added to samples before analysis. Dead cells were excluded with propidium iodide (1 μg/mL; Sigma-Aldrich). Paraformaldehyde-fixed dead cells were excluded with the LIVE/DEAD Fixable Near-IR Dead Cell Stain Kit (Thermo Fisher Scientific).

The following antibodies from BD Biosciences, BioLegend, Invitrogen, or eBioscience were used for flow cytometry: phycoerythrin (PE) or peridinin-chlorophyll cyanine 5.5 (PerCP-Cy5.5)–conjugated CD3 (BD Biosciences, catalog no. 553063, RRID:AB_394596; BD Biosciences, catalog no. 551163, RRID:AB_394082); PE, BUV805, PerCP-Cy5.5, or phycoerythrin-cyanine 7 (PE-Cy7)–conjugated CD4 (BD Biosciences, catalog no. 553049, RRID:AB_394585; BD Biosciences, catalog no. 741912, RRID:AB_2871226; BD Biosciences, catalog no. 550954, RRID:AB_393977; BD Biosciences, catalog no. 561099, RRID:AB_2034007); BV711, Pacific Blue–conjugated (PB), allophycocyanin (APC)-Cy7, or APC-conjugated CD8 (BioLegend, catalog no. 100759, RRID:AB_2563510; BD Biosciences, catalog no. 558106, RRID:AB_397029; BD Biosciences, catalog no. 557654, RRID:AB_396769; BD Biosciences, catalog no. 553035, RRID:AB_398527); BV711-conjugated CD11b (BioLegend, catalog no. 101241, RRID:AB_11218791); APC-conjugated CD11c (BioLegend, catalog no. 117309, RRID:AB_313778); PE-Cy7–conjugated CD19 (BD Biosciences, catalog no. 552854, RRID:AB_394495); PerCP-Cy5.5, PE, or APC-Cy7–conjugated CD25 (BD Biosciences, catalog no. 551071, RRID:AB_394031; BD Biosciences, catalog no. 553866, RRID:AB_395101; BD Biosciences, catalog no. 561038, RRID:AB_2034002); FITC, V450, BUV737, BV786, Alexa Fluor 700,

or PE-Cy7–conjugated CD44 (BD Biosciences, catalog no. 553133, RRID:AB_2076224; BD Biosciences, catalog no. 560451, RRID:AB_1645273; BD Biosciences, catalog no. 612799, RRID:AB_2870126; BD Biosciences, catalog no. 563736, RRID:AB_2738395; BD Biosciences, catalog no. 560567, RRID:AB_1727480; BD Biosciences, catalog no. 560569, RRID:AB_1727484); APC-conjugated CD45 (Thermo Fisher Scientific, catalog no. 17–0451–83, RRID:AB_469393); BUV395, FITC, V450, APC, or PE-conjugated CD45.1 (BD Biosciences, catalog no. 565212, RRID:AB_2722493; BD Biosciences, catalog no. 553775, RRID:AB_395043; BD Biosciences, catalog no. 560520, RRID:AB_1727490; BD Biosciences, catalog no. 558701, RRID:AB_1645214; BD Biosciences, catalog no. 553776, RRID:AB_395044); FITC, PE, or PerCP-Cy5.5–conjugated CD45.2 (BD Biosciences, catalog no. 553772, RRID:AB_395041; BD Biosciences, catalog no. 560695, RRID:AB_1727493; BD Biosciences, catalog no. 561096, RRID:AB_2034008); biotinylated CD49d (BD Biosciences, catalog no. 557419, RRID:AB_396692); APC, BV421, BV786, or PE-conjugated CD62L (BD Biosciences, catalog no. 553152, RRID:AB_398533; BioLegend, catalog no. 104435, RRID:AB_10900082; BD Biosciences, catalog no. 564109, RRID:AB_2738598; BD Biosciences, catalog no. 553151, RRID:AB_394666); V450-conjugated CD69 (BD Biosciences, catalog no. 560690, RRID:AB_1727511); FITC or PE-Cy7–conjugated CD279 (BioLegend, catalog no. 135213, RRID:AB_10689633; BioLegend, catalog no. 135216, RRID:AB_10689635); PE-Cy7 or BV711-conjugated CD366 (Thermo Fisher Scientific, catalog no. 25–5870–80, RRID:AB_2573482; BioLegend, catalog no. 119727, RRID:AB_2716208); FITC or APC-Cy7–conjugated B220 (BD Biosciences, catalog no. 553088, RRID:AB_394618; BD Biosciences, catalog no. 552094, RRID:AB_394335); Brilliant Violet 421 (BV421)–conjugated TCR-β (H57–597; BioLegend, catalog no. 109229, RRID:AB_10933263); PE-Cy7–conjugated NK1.1 (PK136; BD Biosciences, catalog no. 552878, RRID:AB_394507); APC-Cy7–conjugated Ly6C (BD Biosciences, catalog no. 560596, RRID:AB_1727555); PE-conjugated Ly6G (BD Biosciences, catalog no. 551461, RRID:AB_394208); APC or PE-conjugated F4/80 (BD Biosciences, catalog no. 566787, RRID:AB_2869866; BD Biosciences, catalog no. 565410, RRID:AB_2687527); APC-conjugated KLRG1 (Thermo Fisher Scientific, catalog no. 17–5893–82, RRID:AB_469469); PE-Cy7–conjugated IFNγ (BD Biosciences, catalog no. 557649, RRID:AB_396766); FITC or APC-conjugated TNF (BD Biosciences, catalog no. 554418, RRID:AB_395379; BD Biosciences, catalog no. 561062, RRID:AB_2034022); Alexa Fluor 647–conjugated GZMB (BioLegend, catalog no. 515405, RRID:AB_2294995), APC-conjugated T-bet (BioLegend, catalog no. 644813, RRID:AB_10896913); Alexa Fluor 488–conjugated Eomes (Thermo Fisher Scientific, catalog no. 53–4875–80, RRID:AB_10853025), and Alexa Fluor 647–conjugated BCL2 (BioLegend, catalog no. 633510, RRID:AB_2274702). PE-Cy7–conjugated streptavidin was used to detect biotinylated CD49d (9C10).

TCR Signaling

Naïve ($CD44^{lo}CD62L^{hi}$) $CD8^+$ T cells were purified using the EasySep Mouse Naïve $CD8^+$ T Cell Isolation Kit (StemCell Technologies) according to the manufacturer's instructions. Naïve $CD8^+$ T cells were incubated with anti-CD3ε (5 μg/mL) for 15 minutes on ice in RPMI 1640 supplemented with 1% (v/v) FBS. Cells were washed with RPMI 1640 and then incubated with 20 μg/mL rabbit anti-hamster IgG (H+L; Sigma-Aldrich) in RPMI 1640 for the indicated times at 37°C. Cells were washed with ice-cold PBS and lysed in ice-cold RIPA lysis buffer [50 mmol/L HEPES pH 7.4, 1% (v/v) Triton X-100, 1% (v/v) sodium deoxycholate, 0.1% (v/v) SDS, 150 mmol/L NaCl, 10% (v/v) glycerol, 1.5 mmol/L $MgCl_2$, 1 mmol/L EGTA, 50 mmol/L sodium fluoride, 1 μg/mL pepstatin A, 5 μg/mL aprotinin, 1 mmol/L benzamadine, 1 mmol/L phenylmethysulfonylfluoride, and 1 mmol/L sodium vanadate], clarified by centrifugation (16,000 × *g*, 10 minutes, 4°C), and processed for immunoblotting.

To assess intracellular ERK1/2 T185Y187 phosphorylation (p-ERK1/2) by flow cytometry, 3×10^6 T cells isolated from inguinal, brachial, axillary, superficial cervical, and deep cervical lymph nodes were incubated with anti-CD3ε (1 or 5 μg/mL) for 15 minutes on ice in RPMI 1640 supplemented with 1% (v/v) FBS. Cells were washed with RPMI 1640 and then incubated with 20 μg/mL rabbit anti-hamster IgG (H+L; Sigma-Aldrich) in RPMI 1640 for the indicated times at 37°C. Cells were stained with fluorophore-conjugated antibodies against CD4, CD8, CD44, and CD62L; fixed in 2% (w/v) paraformaldehyde; permeabilized with 90% (v/v) methanol; and then intracellularly stained with anti–phospho-p44/42 MAPK (Erk1/2; Cell Signaling Technology) for 30 minutes at room temperature and then with secondary antibodies against rabbit IgG (H+L) $F(ab')_2$ fragment conjugated to Alexa Fluor 647 (Jackson ImmunoResearch Laboratories, catalog no. 111–606–003, RRID:AB_2338079). p-ERK1/2 mean fluorescence intensities (MFI) in $CD4^+$ and $CD8^+$ T-cell subsets were analyzed by flow cytometry.

To assess calcium flux after TCR stimulation, T cells isolated from inguinal, brachial, axillary, superficial cervical, and deep cervical lymph nodes were stained with fluorophore-conjugated antibodies against CD8, CD44, and CD62L and then incubated with 5 μmol/L Fluo-4 AM (Molecular Probes) for 15 minutes at 37°C. T cells were washed three times in complete T-cell medium [RPMI 1640 supplemented with 10% (v/v) FBS, L-glutamine (2 mmol/L), penicillin (100 U/mL)/streptomycin (100 μg/mL), MEM nonessential amino acids (0.1 mmol/L), sodium pyruvate (1 mmol/L), HEPES (10 mmol/L), and 2-β-mercaptoethanol (50 μmol/L)] and incubated with anti-CD3ε (1 μg/mL) for 15 minutes on ice in RPMI 1640 supplemented with 1% (v/v) FBS. Cells were washed with RPMI 1640 supplemented with 1% (v/v) FBS, 20 μg/mL rabbit anti-hamster IgG (H+L; Sigma-Aldrich) was added, and the median calcium response at 37°C was acquired immediately using a BD FACSAria II. Peak time, slope, and peak intensity of the calcium response in $CD8^+$ T-cell subsets were calculated using FlowJo10 (Tree Star Inc.) software.

Cytokine Signaling

For assessing IL15-induced TYK2 and STAT5 phosphorylation in $CD8^+$ central memory T cells, total $CD8^+$ T cells were first enriched using the EasySep Mouse $CD8^+$ T Cell Isolation Kit (StemCell Technologies) and then $CD8^+CD44^{hi}CD62L^{hi}$ central memory T cells were purified by FACS. Purified central memory T cells (4×10^5) in RPMI plus 1% (v/v) FBS were stimulated with human IL15 (50 ng/mL) for the indicated times at 37°C. Cells were washed with ice-cold PBS and lysed in RIPA lysis buffer, clarified by centrifugation (16,000 × *g*, 10 minutes, 4°C), and processed for immunoblotting.

For assessing IL2-induced TYK2 and STAT5 phosphorylation in *in vitro*–generated $CD8^+$ rested effector T cells by immunoblotting, naïve ($CD44^{lo}CD62L^{hi}$) $CD8^+$ T cells were purified using the EasySep Mouse Naïve $CD8^+$ T Cell Isolation Kit (StemCell Technologies) and stimulated with plate-bound anti-CD3 (5 μg/mL) and anti-CD28 (5 μg/mL) for 72 hours at 37°C in complete T-cell medium in the presence of human IL2 (10 ng/mL), washed, and then further expanded for 2 additional days in the presence of human IL2 (10 ng/mL) and murine IL7 (0.2 ng/mL). Activated $CD8^+$ T cells were then rested overnight in RPMI 1640 supplemented with 1% (v/v) FBS in the presence of murine IL7 (0.2 ng/mL). Rested effector $CD8^+$ T cells were stimulated with human IL2 (5 ng/mL) for the indicated times at 37°C. Cells were washed with ice-cold PBS, lysed in RIPA lysis buffer, clarified by centrifugation (16,000 × *g*, 10 minutes, 4°C), and processed for immunoblotting.

For IL2 pulse/chase experiments, *in vitro*–generated $CD8^+$ rested effector T cells were serum-starved in RPMI 1640 supplemented with 0.1% (v/v) FBS for 3 hours, pulsed with 5 ng/mL human IL2 for 10 minutes at 37°C, washed, and then incubated in RPMI 1640 supplemented with 0.1% FBS with or without ruxolitinib (250 nmol/L)

for the indicated times at 37°C. Cells were washed with ice-cold PBS, lysed in RIPA lysis buffer, clarified by centrifugation (16,000 × *g*, 10 minutes, 4°C), and processed for immunoblotting.

For assessing IL2-induced STAT5 phosphorylation in CD8$^+$ rested effector cells by flow cytometry, T cells isolated from inguinal, brachial, axillary, superficial cervical, and deep cervical lymph nodes were stimulated with plate-bound anti-CD3 (5 μg/mL) and anti-CD28 (5 μg/mL) for 72 hours at 37°C in the presence of human IL2 (10 ng/mL). Activated CD8$^+$ T cells were rested overnight in RPMI 1640 supplemented with 1% (v/v) FBS. Rested effector CD8$^+$ T cells were then stimulated with human IL2 (5 ng/mL) for the indicated time points at 37°C. T cells were stained with fluorophore-conjugated antibodies against CD4 and CD8, fixed in 2% (w/v) paraformaldehyde, permeabilized with acetone/methanol (50:50), and then stained intracellularly with anti–p-(Y694) STAT5 (D47E7) XP followed by secondary antibodies against rabbit IgG (H+L) F(ab′)$_2$ fragment conjugated to Alexa Fluor 647 (Jackson ImmunoResearch Laboratories, catalog no. 111–606–003, RRID:AB_2338079). p-ERK1/2 MFIs in rested effector CD8$^+$ T cells were analyzed by flow cytometry.

T-cell Proliferation

T cells isolated from inguinal, brachial, axillary, superficial cervical, and deep cervical lymph nodes were stained with fluorochrome-conjugated antibodies for CD8, CD62L, and CD44 and naïve CD8$^+$CD44^{lo}CD62L^{hi} T cells purified by FACS. For assessing *ex vivo* T-cell proliferation by CTV (Molecular Probes, Thermo Fisher Scientific) dilution, T cells were incubated with CTV in D-PBS at a final concentration of 2 μmol/L for 10 minutes at 37°C. Cells were then washed three times with D-PBS supplemented with 10% (v/v) FBS. T cells (2×10^5) were incubated with the indicated amounts of anti-CD3 and anti-CD28 coated onto 96-well round-bottom plates for 3 days in complete T-cell medium at 37°C, and proliferation was determined by assessing CTV dilution by flow cytometry. For cell quantification, a known number of Calibrite Beads (BD Biosciences) or Nile Red Beads (Prositech) or Flow-Count Fluorospheres (Beckman Coulter) were added to samples before analysis.

For assessing OT-I T-cell proliferation *in vivo*, FACS-purified naïve OT-I$^+$ CD8$^+$CD44^{lo}CD62L^{hi} T cells were labeled with 5 μmol/L CTV and adoptively transferred (2×10^6) into female Ly5.1 mice bearing established AT3-OVA tumors (40–50 mm^2). On day 8 after adoptive transfer, T cells were harvested from draining lymph nodes and stained with fluorophore-conjugated antibodies against CD8, CD45.1 (Ly5.1), and CD45.2 (Ly5.2) and the proliferation of CD8$^+$Ly5.1$^-$Ly5.2$^+$ T cells was determined by flow cytometry.

Tumor Studies

Male mice were injected subcutaneously with 1×10^5 B16F10 or B16F10-OVA cells or 5×10^5 MC38 or MC38-OVA tumor cells resuspended in 100 μL D-PBS into the flank. Alternatively, female mice were injected orthotopically with 5×10^5 AT3 or AT3-OVA cells resuspended in 20 μL D-PBS into the fourth mammary fat pad.

For CAR T-cell studies, female human HER2 TG mice were injected orthotopically with 2×10^5 HER2-E0771 cells resuspended in 20 μL D-PBS into the fourth mammary fat pad. At day 7 after tumor cell injection, human HER2 TG mice were preconditioned with total body irradiation (4 Gy) prior to the adoptive transfer of 2×10^7 CAR T cells. Tumor sizes were measured in two dimensions (mm^2) using electronic calipers three times per week as soon as the tumors were palpable (20–25 mm^2). Mice were sacrificed at the ethical experimental endpoint (200 mm^2 tumor size), and individual tumors were removed to measure tumor weights or to assess T-cell infiltrates by flow cytometry.

Histology and IHC

For IHC, tumors were formalin-fixed and paraffin-embedded. Sections were dewaxed in Histopure (CSA Pathology) for 3 × 5 minutes and dehydrated in ethanol (3 × 5 minutes), and antigens were retrieved in Tris/EDTA pH 8.0 buffer for 5 minutes in a pressure cooker (70 kpa). Endogenous peroxidase activity was blocked in 3% H_2O_2 for 10 minutes, and sections were blocked with 1.5% (v/v) horse (for Ki-67) or goat (for cleaved caspase-3) serum in PBS for 30 minutes at room temperature and incubated overnight (4°C) with primary antibodies anti-Ki67 (1:400; Cell Signaling Technology, catalog no. 9449, RRID:AB_2797703) or anti–cleaved caspase-3 (Asp175; 1:2,000; Cell Signaling Technology, catalog no. 9664, RRID:AB_2070042). Ki67- or cleaved caspase-3–positive cells were visualized using mouse (Ki-67) or rabbit (cleaved caspase-3) IgG VECTORSTAIN ABC Elite and DAB (3,3′-diaminobenzidine) Peroxidase Substrate Kits (Vector Laboratories) and counterstained with hematoxylin. TUNEL staining was performed using the DeadEndColorimetric TUNEL System (Promega) following the manufacturer's instructions. Sections were visualized on an Olympus CX33 microscope (Olympus) and imaged at 20× magnification.

For immunofluorescence microscopy, tumors were formalin-fixed and paraffin-embedded. Sections were dewaxed in Histopure (CSA Pathology) for 3 × 5 minutes and dehydrated in ethanol (3 × 5 minutes), and antigens were retrieved in Leica EDTA epitope pH 9 retrieval buffer (Leica Biosystems) for 5 minutes in a pressure cooker (70 kpa). Sections were blocked in 5% normal goat serum in Tris-buffered saline for 60 minutes at room temperature and incubated overnight (4°C) with endomucin primary antibody (1:200; Thermo Fisher Scientific, catalog no. 14–5851–82, RRID:AB_891527) and then with goat anti-rat IgG Alexa Fluor 555 (Thermo Fisher Scientific, catalog no. A-21434, RRID:AB_2535855) secondary antibody for 60 minutes at room temperature. Nuclei were counterstained with DAPI before mounting in Fluoromount-G mounting medium (Thermo Fisher Scientific). Fluorescence was visualized on a Zeiss Axioskop-2 Mot Plus fluorescence microscope (Zeiss) at 20× magnification.

For brain histology, mice were transcardially perfused with heparinized saline [10,000 U/L heparin in 0.9% (w/v) NaCl] followed by 4% (w/v) paraformaldehyde in PBS (PBS; 0.1 mol/L, pH 7.4). Brains were postfixed overnight at 4°C and then refrigerated for 3 days in 30% (w/v) sucrose in 0.1 mol/L PBS to cryoprotect the tissue before freezing on dry ice. Series of 30-μm sections (180 μm apart) were cut in the coronal plane (Leica CM1850 Cryostat, Leica Biosystems) throughout the entire rostral–caudal extent of the cerebellum. A representative subset of sections were stained with hematoxylin and eosin, mounted with dibutylphthalate polystyrene xylene mounting media, and imaged on an Olympus CX33 microscope (Olympus) at 20× magnification.

Generation of Murine CAR T Cells

Murine CAR T cells were generated as previously described (11). Briefly, splenocytes were cultured overnight with anti-CD3ε (0.5 μg/mL) and anti-CD28 (0.5 μg/mL) in the presence of 10 ng/mL human IL2 and 0.2 ng/mL murine IL7 in complete T-cell medium. Retroviruses encoding a second-generation CAR targeting HER2 were obtained from the supernatant of the GP+E86 packaging line spun together with T cells onto RetroNectin-coated (10 μg/mL) 6-well plates (Takara Bio) and incubated overnight before the second viral transduction. T cells were maintained in IL2/IL7-containing complete media and used 7 to 8 days after transduction.

CAR T-cell Cytotoxicity Assays

For CAR T-cell cytotoxicity assays, HER2-expressing 24JK sarcoma cells (HER2-24JK) and HER2-negative 24JK sarcoma cells were labeled with 5 μmol/L or 0.5 μmol/L CTV (Invitrogen Molecular Probes), respectively, in D-PBS supplemented with 0.1% (v/v) BSA

for 15 minutes at 37°C. Tumor cells were then washed three times with D-PBS supplemented with 10% (v/v) FBS and mixed at a 1:1 ratio. HER2-specific CAR T cells were added at different concentrations to HER2-expressing (5×10^4) and HER2-negative (5×10^4) 24JK cells and incubated for 4 hours at 37°C in complete T-cell medium. Antigen-specific target cell lysis, assessed by the specific depletion of CTV^{hi} HER2-24JK cells, but not CTV^{dim} 24JK cells, was monitored by flow cytometry.

PTP1B Inhibition and Immune Checkpoint Blockade

Mice with established tumors (40–50 mm^2) were randomly grouped to receive 0.9% (w/v) saline only or MSI-1436 dissolved in 0.9% (w/v) saline. MSI-1436 was administered at 5 or 10 mg/kg body weight in 100 µL every third day intraperitoneally for up to 29 days. Control animals received an injection at the same time of 100 µL of saline. Solutions were freshly prepared before each administration. Mice were sacrificed at the experimental endpoint (200 mm^2 tumor size), and individual tumors were removed to measure tumor weights or to assess T-cell infiltrates by flow cytometry.

To assess the combined effects of PTP1B inhibition with MSI-1436 and immune checkpoint blockade with anti–PD-1, tumor-bearing mice (40–50 mm^2) were treated with MSI-1436 as described above every third day. In addition, mice received four intraperitoneal injections of anti–PD-1 (200 µg in 200 µL D-PBS; clone RMP1–14) or rat IgG2a isotype control (100 µg in 200 µL D-PBS, Bio X Cell) every 4 days for up to 27 days. Mice were sacrificed at the experimental endpoint (200 mm^2 tumor size), and individual tumors were removed to measure tumor weights or to assess T-cell infiltrates by flow cytometry.

Adoptive OT-I T-cell Therapy

Female Ly5.1 mice were injected orthotopically with 5×10^5 AT3-OVA cells resuspended in 20 µL D-PBS into the fourth mammary fat pad. At day 7 to 12 after tumor injection, mice with established tumors (40–50 mm^2) were randomly grouped and 2×10^6 naïve $Ly5.2^+CD8^+CD44^{lo}CD62L^{hi}$ OT-I T cells [purified by FACS or using the EasySep murine naïve $CD8^+$ T Cell Isolation Kit (StemCell Technologies)] were injected intravenously. Mice were sacrificed at the indicated times, and $Ly5.1^-Ly5.2^+CD8^+$ OT-I T-cell infiltrates in draining lymph nodes, spleens, and tumors were determined by flow cytometry.

Analysis of Tumor-Infiltrating T Cells

Tumor-bearing mice were sacrificed, and tumors excised and digested at 37°C for 30 minutes using a cocktail of 1 mg/mL collagenase type IV (Worthington Biochemicals) and 0.02 mg/mL DNase (Sigma-Aldrich) in DMEM supplemented with 2% (v/v) FBS. Cells were passed through a 70-µm cell strainer (BD Biosciences) twice and processed for flow cytometry. For the assessment of activated and exhausted T cells, cells were surface stained with fluorophore-conjugated antibodies against CD62L, CD44, PD-1, and TIM3. For the detection of the intracellular cytokines TNF and IFNγ, T cells were stimulated with phorbol 12-myristate 13-acetate (PMA; 20 ng/mL; Sigma-Aldrich) and ionomycin (1 µg/mL; Sigma-Aldrich) in the presence of GolgiPlug and GolgiStop (BD Biosciences) for 4 hours at 37°C in complete T-cell medium. For the intracellular detection of GZMB, cells were processed untreated without the addition of GolgiPlug and GolgiStop.

CRISPR Ribonucleoprotein Gene Editing

PTP1B was deleted in AT3-OVA cells using CRISPR ribonucleoprotein (RNP)-based gene editing. AT3-OVA tumor cells were electroporated with recombinant Cas9 (74 pmol; Alt-R S.p. Cas9 Nuclease V3, Integrated DNA Technologies) precomplexed with either synthetic single-guide (sg) RNAs (600 pmol) targeting *Ptpn1* (5′UUUCAGUU GACCACAGU3′), or nontargeting sgRNAs (5′GCACUACCAGAGC UAACUCA3′) as a control, using the P3 Primary Cell 4D-Nucleofector X Kit (Lonza Bioscience) and cultured in high-glucose DMEM supplemented with 10% (v/v) FBS, L-glutamine (2 mmol/L), penicillin (100 U/mL)/streptomycin (100 µg/mL), and HEPES (10 mmol/L).

For deleting PTP1B in human T cells, human PBMCs were isolated from normal buffy coats using Ficoll centrifugation and cultured in complete human T-cell medium [RPMI 1640 (Gibco Life Technologies) supplemented with 10% heat-inactivated FBS, L-glutamine (2 mmol/L), MEM nonessential amino acids (0.1 mmol/L), sodium pyruvate (1 mmol/L), 10 mmol/L HEPES, 100 U/mL penicillin, and 100 µg/mL streptomycin] supplemented with human IL2 (300 IU/mL) and stimulated with soluble anti-human CD3 (OKT3; 30 ng/mL, Thermo Fisher Scientific, catalog no. 14–0037–80, RRID:AB_467056) for 3 days at 37°C. Activated human T cells were then electroporated, as described for AT3-OVA cells, with recombinant Cas9 precomplexed with either sgRNAs targeting human *PTPN1* (5′UAAAAAUGGAA GAAGCCCAA3′) or nontargeting sgRNAs (5′GCACUACCA GAGC UAACUCA3′) using the P3 Primary Cell 4D-Nucleofector X Kit according to the manufacturer's instructions.

Analysis of Human T Cells

To monitor for the TCR-mediated activation of human PBMC-derived T cells, control or PTP1B-deleted T cells were cultured with plate-bound anti-human CD3 (OKT3; 30 ng/mL, Thermo Fisher Scientific, catalog no. 14–0037–80, RRID:AB_467056) in complete human T-cell media overnight and then stained with anti-human CD8-FITC (Miltenyi Biotec, catalog no. 130–080–601, RRID:AB_244336), anti-human CD4-PE-Cy7 (BD Biosciences, catalog no. 557852, RRID:AB_396897), and anti-human CD69-APC (BD Biosciences, catalog no. 555533, RRID:AB_398602) and analyzed by flow cytometry. For assessing the human T-cell proliferation, T cells were incubated with CTV in D-PBS supplemented with BSA (0.1%) at a final concentration of 2 µmol/L for 10 minutes at 37°C. Cells were then washed three times with D-PBS supplemented with 10% (v/v) FBS. Washed T cells (1×10^5) were incubated with plate-bound anti-human CD3 (0–1 µg/mL) antibody for 5 days at 37°C and then harvested and stained with anti-human CD8-FITC (Miltenyi Biotec, catalog no. 130–080–601, RRID:AB_244336) and anti-human CD4-PE-Cy7 (BD Biosciences, catalog no. 557852, RRID:AB_396897), and proliferation was assessed by monitoring for CTV dilution by flow cytometry.

For assessing STAT5 signaling, human T cells were fixed in 4% (v/v) paraformaldehyde, permeabilized with methanol/acetone (50/50) and then stained intracellularly with rabbit anti-human p-(Y694) STAT5 (D47E7) XP (Cell Signaling Technology, catalog no. 4322, RRID:AB_10544692), mouse anti-BCL2 (Santa Cruz Biotechnology, catalog no. sc-509, RRID:AB_626733) or mouse anti–BCL-xL (Santa Cruz Biotechnology, catalog no. sc-8392, RRID:AB_626739) for 60 minutes and then with anti-rabbit IgG (H+L) $F(ab')_2$ fragment conjugated to Alexa Fluor 647 (Jackson ImmunoResearch Laboratories, catalog no. 111–606–003, RRID:AB_2338079) or anti-mouse IgG (H+L) conjugated to Alexa Fluor 647 (Thermo Fisher Scientific, catalog no. A-21235, RRID:AB_2535804) secondary antibodies. Cells were then stained with anti-human CD8-FITC (Miltenyi Biotec, catalog no. 130–080–601, RRID:AB_244336) and anti-human CD4-PE-Cy7 (BD Biosciences, catalog no. 557852, RRID:AB_396897), and MFIs for p-(Y694) STAT5, BCL-xL, and BCL2 in $CD4^+$ and $CD8^+$ T-cell subsets were determined by flow cytometry.

Quantitative Real-Time PCR

RNA was extracted with TRIzol reagent (Thermo Fisher Scientific), and RNA quality and quantity were determined using a NanoDrop 2000 (Thermo Fisher Scientific). mRNA was reverse transcribed with the High-Capacity cDNA Reverse Transcription Kit (Applied Biosystems) and processed for quantitative real-time PCR using the Fast SYBR Green Master Mix (Applied Biosystems). Primer sets from PrimePCR SYBR Green Assay (Bio-Rad, catalog no. 10025636) were utilized to perform quantitative PCR detecting *Ptpn1* (Bio-Rad PrimePCR SYBR

Green Assay: qMmuCED0045967). Relative gene expression (ΔΔCt) was determined by normalization to the housekeeping gene *Rps18*.

Human and Animal Ethics

Human ethics approval for the use of PBMCs was granted by both the Australian Red Cross Blood Services and the Peter MacCallum Cancer Centre Human Research and Ethics committee (HREC# 01/14). Informed written consent was obtained from blood donors by the Australian Red Cross, and the studies were conducted in accordance with the Australian Code for the Responsible Conduct of Research and the National Statement on Ethical Conduct in Human Research (National Health and Medical Research Council Act 1992).

All animal experiments were performed in accordance with the National Health and Medical Research Council Australian Code of Practice for the Care and Use of Animals. All protocols were approved by the Monash University School of Biomedical Sciences Animal Ethics Committee (Ethics numbers: MARP/2012/124, 23177, and 27792) or the Peter MacCallum Animal Ethics and Experimentation Committee (Ethics number: E604).

Statistical Analyses

Statistical analyses were performed with GraphPad Prism software 9 using the nonparametric two-tailed Mann–Whitney *U* test, the parametric two-tailed Student *t* test, the one-way or two-way ANOVA test using Kruskal–Wallis, Tukey, Bonferroni, or Sidak *post hoc* comparison, or the log-rank (Mantel–Cox test) where indicated. *, $P < 0.05$; **, $P < 0.01$; ***, $P < 0.001$; and ****, $P < 0.0001$ were considered significant.

Data Availability

The datasets generated during and/or analyzed during this study are available from the corresponding author on reasonable request.

Authors' Disclosures

F. Wiede reports grants from the National Health and Medical Research Council of Australia during the conduct of the study, as well as a patent for PCT/AU2019/050565 pending to Monash University and Peter MacCallum Cancer Centre. P.A. Beavis reports grants from AstraZeneca, Gilead Sciences, and Bristol Myers Squibb outside the submitted work. P.K. Darcy reports other support from Prescient Therapeutics, Myeloid Therapeutics, and Bristol Myers Squibb outside the submitted work. N.K. Tonks reports personal fees from DepYmed, Inc. outside the submitted work. T. Tiganis reports grants from the National Health and Medical Research Council of Australia during the conduct of the study; personal fees and nonfinancial support from DepYmed, Inc. outside the submitted work; a patent for PCT/AU2019/050565 pending; and is on the scientific advisory board for DepYmed, Inc. No disclosures were reported by the other authors.

Authors' Contributions

F. Wiede: Investigation, methodology, writing–review and editing. **K.-H. Lu:** Investigation, methodology, writing–review and editing. **X. Du:** Investigation, methodology, writing–review and editing. **M.N. Zeissig:** Investigation, methodology, writing–review and editing. **R. Xu:** Investigation, writing–review and editing. **P.K. Goh:** Investigation, methodology, writing–review and editing. **C.E. Xirouchaki:** Investigation, methodology, writing–review and editing. **S.J. Hogarth:** Investigation, methodology, writing–review and editing. **S. Greatorex:** Investigation, methodology, writing–review and editing. **K. Sek:** Investigation, methodology, writing–review and editing. **R.J. Daly:** Resources, writing–review and editing. **P.A. Beavis:** Resources, writing–review and editing. **P.K. Darcy:** Resources, writing–review and editing. **N.K. Tonks:** Resources, funding acquisition, writing–review and editing. **T. Tiganis:** Conceptualization, formal analysis, supervision, funding acquisition, validation, writing–original draft, project administration, writing–review and editing.

Acknowledgments

We thank Alexandra Ziegler for technical support, Axel Kallies for critical review of the manuscript, and DepYmed, Inc. for providing MSI1436. This work was supported by the National Health and Medical Research Council (NHMRC) of Australia (to T. Tiganis and F. Wiede) and the NIH (CA53840; to N.K. Tonks).

The costs of publication of this article were defrayed in part by the payment of page charges. This article must therefore be hereby marked *advertisement* in accordance with 18 U.S.C. Section 1734 solely to indicate this fact.

Received May 28, 2021; revised October 1, 2021; accepted November 15, 2021; published first November 18, 2021.

REFERENCES

1. Topalian SL, Drake CG, Pardoll DM. Immune checkpoint blockade: a common denominator approach to cancer therapy. Cancer Cell 2015;27:450–61.
2. Blank CU, Haining WN, Held W, Hogan PG, Kallies A, Lugli E, et al. Defining 'T cell exhaustion.' Nat Rev Immunol 2019;19:665–74.
3. Sharma P, Hu-Lieskovan S, Wargo JA, Ribas A. Primary, adaptive, and acquired resistance to cancer immunotherapy. Cell 2017;168:707–23.
4. Zappasodi R, Merghoub T, Wolchok JD. Emerging concepts for immune checkpoint blockade-based combination therapies. Cancer Cell 2018;33:581–98.
5. Celis-Gutierrez J, Blattmann P, Zhai Y, Jarmuzynski N, Ruminski K, Gregoire C, et al. Quantitative interactomics in primary T cells provides a rationale for concomitant PD-1 and BTLA coinhibitor blockade in cancer immunotherapy. Cell Rep 2019;27:3315–30.
6. Patsoukis N, Wang Q, Strauss L, Boussiotis VA. Revisiting the PD-1 pathway. Sci Adv 2020;6:eabd2712.
7. Wiede F, Shields BJ, Chew SH, Kyparissoudis K, van Vliet C, Galic S, et al. T cell protein tyrosine phosphatase attenuates T cell signaling to maintain tolerance in mice. J Clin Invest 2011;121:4758–74.
8. Wiede F, La Gruta NL, Tiganis T. PTPN2 attenuates T-cell lymphopenia-induced proliferation. Nat Commun 2014;5:3073.
9. Wiede F, Sacirbegovic F, Leong YA, Yu D, Tiganis T. PTPN2-deficiency exacerbates T follicular helper cell and B cell responses and promotes the development of autoimmunity. J Autoimmun 2017;76:85–100.
10. Wiede F, Brodnicki TC, Goh PK, Leong YA, Jones GW, Yu D, et al. T-cell-specific PTPN2 deficiency in NOD mice accelerates the development of type 1 diabetes and autoimmune comorbidities. Diabetes 2019;68:1251–66.
11. Wiede F, Lu KH, Du X, Liang S, Hochheiser K, Dodd GT, et al. PTPN2 phosphatase deletion in T cells promotes anti-tumour immunity and CAR T-cell efficacy in solid tumours. EMBO J 2020;39:e103637.
12. LaFleur MW, Nguyen TH, Coxe MA, Miller BC, Yates KB, Gillis JE, et al. PTPN2 regulates the generation of exhausted CD8(+) T cell subpopulations and restrains tumor immunity. Nat Immunol 2019;20:1335–47.
13. Tiganis T. PTP1B and TCPTP - nonredundant phosphatases in insulin signaling and glucose homeostasis. FEBS J 2013;280:445–58.
14. Loh K, Fukushima A, Zhang X, Galic S, Briggs D, Enriori PJ, et al. Elevated hypothalamic TCPTP in obesity contributes to cellular leptin resistance. Cell Metab 2011;14:684–99.
15. Dodd GT, Decherf S, Loh K, Simonds SE, Wiede F, Balland E, et al. Leptin and Insulin Act on POMC neurons to promote the browning of white fat. Cell 2015;160:88–104.
16. Elchebly M, Wagner J, Kennedy TE, Lanctot C, Michaliszyn E, Itie A, et al. Neuroendocrine dysplasia in mice lacking protein tyrosine phosphatase sigma. Nat Genet 1999;21:330–3.
17. Klaman LD, Boss O, Peroni OD, Kim JK, Martino JL, Zabolotny JM, et al. Increased energy expenditure, decreased adiposity, and tissue-specific insulin sensitivity in protein-tyrosine phosphatase 1B-deficient mice. Mol Cell Biol 2000;20:5479–89.

18. Zhang ZY, Dodd GT, Tiganis T. Protein Tyrosine Phosphatases in Hypothalamic Insulin and Leptin Signaling. Trends Pharmacol Sci 2015;36:661–74.
19. Krishnan N, Koveal D, Miller DH, Xue B, Akshinthala SD, Kragelj J, et al. Targeting the disordered C terminus of PTP1B with an allosteric inhibitor. Nat Chem Biol 2014;10:558–66.
20. Lantz KA, Hart SG, Planey SL, Roitman MF, Ruiz-White IA, Wolfe HR, et al. Inhibition of PTP1B by trodusquemine (MSI-1436) causes fat-specific weight loss in diet-induced obese mice. Obesity (Silver Spring) 2010;18:1516–23.
21. Krishnan N, Krishnan K, Connors CR, Choy MS, Page R, Peti W, et al. PTP1B inhibition suggests a therapeutic strategy for Rett syndrome. J Clin Invest 2015;125:3163–77.
22. Julien SG, Dube N, Read M, Penney J, Paquet M, Han Y, et al. Protein tyrosine phosphatase 1B deficiency or inhibition delays ErbB2-induced mammary tumorigenesis and protects from lung metastasis. Nat Genet 2007;39:338–46.
23. Bentires-Alj M, Neel BG. Protein-tyrosine phosphatase 1B is required for HER2/Neu-induced breast cancer. Cancer Res 2007;67:2420–4.
24. Hoekstra E, Das AM, Swets M, Cao W, van der Woude CJ, Bruno MJ, et al. Increased PTP1B expression and phosphatase activity in colorectal cancer results in a more invasive phenotype and worse patient outcome. Oncotarget 2016;7:21922–38.
25. Penafuerte C, Feldhammer M, Mills JR, Vinette V, Pike KA, Hall A, et al. Downregulation of PTP1B and TC-PTP phosphatases potentiate dendritic cell-based immunotherapy through IL-12/IFNgamma signaling. Oncoimmunology 2017;6:e1321185.
26. Martin-Granados C, Prescott AR, Le Sommer S, Klaska IP, Yu T, Muckersie E, et al. A key role for PTP1B in dendritic cell maturation, migration, and T cell activation. J Mol Cell Biol 2015;7:517–28.
27. Villarino AV, Kanno Y, O'Shea JJ. Mechanisms and consequences of Jak-STAT signaling in the immune system. Nat Immunol 2017;18:374–84.
28. Ross SH, Cantrell DA. Signaling and function of interleukin-2 in T lymphocytes. Annu Rev Immunol 2018;36:411–33.
29. Myers MP, Andersen JN, Cheng A, Tremblay ML, Horvath CM, Parisien JP, et al. TYK2 and JAK2 are substrates of protein-tyrosine phosphatase 1B. J Biol Chem 2001;276:47771–4.
30. Zabolotny JM, Bence-Hanulec KK, Stricker-Krongrad A, Haj F, Wang Y, Minokoshi Y, et al. PTP1B regulates leptin signal transduction in vivo. Dev Cell 2002;2:489–95.
31. Savas P, Salgado R, Denkert C, Sotiriou C, Darcy PK, Smyth MJ, et al. Clinical relevance of host immunity in breast cancer: from TILs to the clinic. Nat Rev Clin Oncol 2016;13:228–41.
32. Chan JD, Lai J, Slaney CY, Kallies A, Beavis PA, Darcy PK. Cellular networks controlling T cell persistence in adoptive cell therapy. Nat Rev Immunol 2021;21:769–84.
33. Jameson SC, Masopust D. Understanding subset diversity in T cell memory. Immunity 2018;48:214–26.
34. Paijens ST, Vledder A, de Bruyn M, Nijman HW. Tumor-infiltrating lymphocytes in the immunotherapy era. Cell Mol Immunol 2021;18:842–59.
35. Sade-Feldman M, Yizhak K, Bjorgaard SL, Ray JP, de Boer CG, Jenkins RW, et al. Defining T cell states associated with response to checkpoint immunotherapy in melanoma. Cell 2018;175:998–1013.
36. Mattarollo SR, Loi S, Duret H, Ma Y, Zitvogel L, Smyth MJ. Pivotal role of innate and adaptive immunity in anthracycline chemotherapy of established tumors. Cancer Res 2011;71:4809–20.
37. Courtney AH, Lo WL, Weiss A. TCR signaling: mechanisms of initiation and propagation. Trends Biochem Sci 2018;43:108–23.
38. Moriggl R, Topham DJ, Teglund S, Sexl V, McKay C, Wang D, et al. Stat5 is required for IL-2-induced cell cycle progression of peripheral T cells. Immunity 1999;10:249–59.
39. Tripathi P, Kurtulus S, Wojciechowski S, Sholl A, Hoebe K, Morris SC, et al. STAT5 is critical to maintain effector CD8$^+$ T cell responses. J Immunol 2010;185:2116–24.
40. Bence KK, Delibegovic M, Xue B, Gorgun CZ, Hotamisligil GS, Neel BG, et al. Neuronal PTP1B regulates body weight, adiposity and leptin action. Nat Med 2006;12:917–24.
41. Mardiana S, Solomon BJ, Darcy PK, Beavis PA. Supercharging adoptive T cell therapy to overcome solid tumor-induced immunosuppression. Sci Transl Med 2019;11:eaaw2293.
42. Haynes NM, Trapani JA, Teng MW, Jackson JT, Cerruti L, Jane SM, et al. Single-chain antigen recognition receptors that costimulate potent rejection of established experimental tumors. Blood 2002;100:3155–63.
43. John LB, Devaud C, Duong CP, Yong CS, Beavis PA, Haynes NM, et al. anti–PD-1 antibody therapy potently enhances the eradication of established tumors by gene-modified T cells. Clin Cancer Res 2013;19:5636–46.
44. Piechocki MP, Ho YS, Pilon S, Wei WZ. Human ErbB-2 (Her-2) transgenic mice: a model system for testing Her-2 based vaccines. J Immunol 2003;171:5787–94.
45. Zabolotny JM, Kim YB, Welsh LA, Kershaw EE, Neel BG, Kahn BB. Protein-tyrosine phosphatase 1B expression is induced by inflammation in vivo. J Biol Chem 2008;283:14230–41.
46. Bertrand F, Rochotte J, Colacios C, Montfort A, Tilkin-Mariame AF, Touriol C, et al. Blocking tumor necrosis factor alpha enhances CD8 T-cell-dependent immunity in experimental melanoma. Cancer Res 2015;75:2619–28.
47. Tam EM, Fulton RB, Sampson JF, Muda M, Camblin A, Richards J, et al. Antibody-mediated targeting of TNFR2 activates CD8$^+$ T cells in mice and promotes antitumor immunity. Sci Transl Med 2019;11:eaax0720.
48. Lu X, Malumbres R, Shields B, Jiang X, Sarosiek KA, Natkunam Y, et al. PTP1B is a negative regulator of interleukin 4-induced STAT6 signaling. Blood 2008;112:4098–108.
49. Zhu Y, Ju S, Chen E, Dai S, Li C, Morel P, et al. T-bet and eomesodermin are required for T cell-mediated antitumor immune responses. J Immunol 2010;185:3174–83.
50. Lynn RC, Weber EW, Sotillo E, Gennert D, Xu P, Good Z, et al. c-Jun overexpression in CAR T cells induces exhaustion resistance. Nature 2019;576:293–300.
51. Carter LL, Fouser LA, Jussif J, Fitz L, Deng B, Wood CR, et al. PD-1: PD-L inhibitory pathway affects both CD4$^+$ and CD8$^+$ T cells and is overcome by IL-2. Eur J Immunol 2002;32:634–43.
52. Walsh SR, Simovic B, Chen L, Bastin D, Nguyen A, Stephenson K, et al. Endogenous T cells prevent tumor immune escape following adoptive T cell therapy. J Clin Invest 2019;129:5400–10.
53. Watanabe N, McKenna MK, Shaw AR, Suzuki M. Clinical CAR-T cell and oncolytic virotherapy for cancer treatment. Mol Ther 2021;29:505–20.
54. Redeker A, Welten SP, Baert MR, Vloemans SA, Tiemessen MM, Staal FJ, et al. The quantity of autocrine IL-2 governs the expansion potential of CD8$^+$ T cells. J Immunol 2015;195:4792–801.